Damage Identification of the Dowling Hall Footbridge Based on Ambient Acceleration and Strain Measurement

A thesis

submitted by

Xiang Li

In partial fulfillment of the requirements
for the degree of

Master of Science

in

Civil and Environmental Engineering

TUFTS UNIVERSITY

August 2013

Thesis Committee:

Assistant Professor Babak Moaveni, Chair

Professor Masoud Sanayei

Assistant Professor Jason Rife

Abstract

This study focuses on detection of physically simulated damage on the Dowling Hall footbridge. A continuous monitoring system has been installed on this footbridge located at Medford campus of Tufts University. The system is equipped with accelerometers and (dynamic) strain gauges that can measure ambient response of the bridge. Damage was simulated on the bridge by loading concrete blocks on segments of the bridge deck. The location and extent of damage (added mass) were estimated using a finite element (FE) model updating method. Modal parameters, such as natural frequencies and mode shapes, were extracted from measured ambient vibration data before and after the addition of mass and used in the FE model updating. Performance of the proposed damage identification method is evaluated using numerically simulated and experimentally measured data. Effects of input factors such as number, locations and types of sensors on the accuracy of damage identification results are investigated.

Acknowledgements

The National Science Foundation under NSF-BRIGE program is acknowledged for support of this study. I would like to offer great gratitude to my advisor Prof. Babak Moaveni for his patient guidance and valuable advices all through this project. I also want to thank the rest of my committee members: Prof. Masoud Sanayei and Prof. Jason Rife for their insightful comments and useful suggestions. Appreciations are given to Iman Behmanesh, Alyssa Kody and Amin Nozari for their direct assistance in this research, including establishment of the finite element model, identification of modal data and accomplishment of the loading test. I am also grateful to Anish KP for his personal help during my two-year study at Tufts University and Michelle Ashley for her proof reading of the thesis. Last but not least, gratitude is given to my family members, especially my parents, Jianming Li (李建明) and Na Li (李娜) for their support and encouragement given to me all through my life.

Table of Contents

List of Tables

List of Figures

Chapter 1 Introduction

1.1 Motivation for Structural Health Monitoring

On May 23, 2013, a heavily travelled bridge collapsed on Interstate 5 over the Skagit River in Washington State. Police claimed that the collapse was directly caused by the collision between a tractor-trailer and one of the bridge's overhead trusses. Aging of the bridge made it unable to stand the hit and a whole span dropped into the river.

Figure 1.1 Collapsed bridge in Washington State (Skift.com)

Recent structural failures like the Washington State Bridge recall the aging problem of the nation's infrastructures and underline the need for improved infrastructure safety inspection and maintenance. America's overall grade for bridges is C^{+}: Mediocre, according to the Report Card for America's Infrastructure in 2013 (ASCE 2013) issued by the American Society of Civil Engineers (ASCE). This nationwide statistic indicates that, approximately one in

nine of the nation's 607,380 bridges are rated as "structurally deficient". It means that these bridges cannot provide the load-carrying capacity and require frequent inspection and significant maintenance. Efforts to estimate these potential threats are essential. The Federal Highway Administration (FHWA) assessment indicates that more than $20 billion should be spent every year to repair and replace the deficient bridges until 2028. ASCE's recommended solutions include increasing government investment for repair to reduce the number of structurally deficient bridges and developing a national strategic plan capable of monitoring and detecting structurally deficient bridges. Visual inspection alone cannot fully satisfy the requirements. In order to truly understand health condition of the nation's bridges, structural health monitoring (SHM) should be implemented.

SHM is defined as the process of damage detection for engineering structures (Brian, 1976). In this definition, any change in structural parameters that can affect the structure's performance, including material properties, geometric deployments and boundary conditions, is considered as "damage". There are four levels of damage identification: (1) detection, to determine whether or not damage exists in the structure; (2) localization, to specify location of the damage whose existence has already been confirmed; (3) quantification, to assess extent of the damage in addition to its existence and location; and (4) prediction of future damage, to estimate the ability of the damaged structure to service functionally and what kind of repair is necessary for the existed damage (Rytter, 1993). Having information about the location and extent of damage makes it possible to provide an early alert if a structure is not safe. Also, the information offers

instructions for improved usage of limited resources for repair and maintenance of deficient structures.

Vibration-based SHM of large-scale civil structures has been widely used over the last decade. The theory behind vibration-based SHM is based on the fact that the dynamic parameters of a structure are functions of its physical properties. Therefore, changes of the structure properties can be detected by comparing vibration characteristics of the damaged and undamaged structure. Sensor-measured vibration data is used to extract dynamic parameters (e.g., natural frequencies and mode shapes) of the structure and hence predict the change in its physical properties (e.g., mass, damping, and stiffness). This study focuses on identification of physically simulated damage on the Dowling Hall footbridge from identified modal parameters.

1.2 Dowling Hall Footbridge

The Dowling Hall Footbridge, as shown in Figure 1.2, is a pedestrian bridge located at Medford campus of Tufts University, Massachusetts. It connects upper Tufts campus on its western side to the 7th floor of Dowling Hall in the east. This two-span continuous bridge is supported by one abutment on the campus-side and two steel and masonry piers. The pier in the mid-span is Pier A, and the other on the eastern side near Dowling Hall is Pier B. The length of each span is 72 ft (22 m) long and width is 12 ft (3.7 m). The structural frame of the bridge is constructed of steel from Hallow Structural Sections (HSS) and the deck is composed of reinforced concrete. The bridge is suitable for vibration-based SHM

because it is flexible. Vibration can be easily excited by pedestrian walk or wind and can be obviously felt with several persons jumping on it.

Figure 1.2 Dowling Hall footbridge (Moser and Moaveni 2013)

1.3 Continuous Monitoring System

A vibration-based continuous monitoring system was designed and installed on the Dowling Hall Footbridge in 2009 and has been recording data continuously since 2010. The system was composed of eight accelerometers and ten thermocouples, as indicated in Figure 1.3.

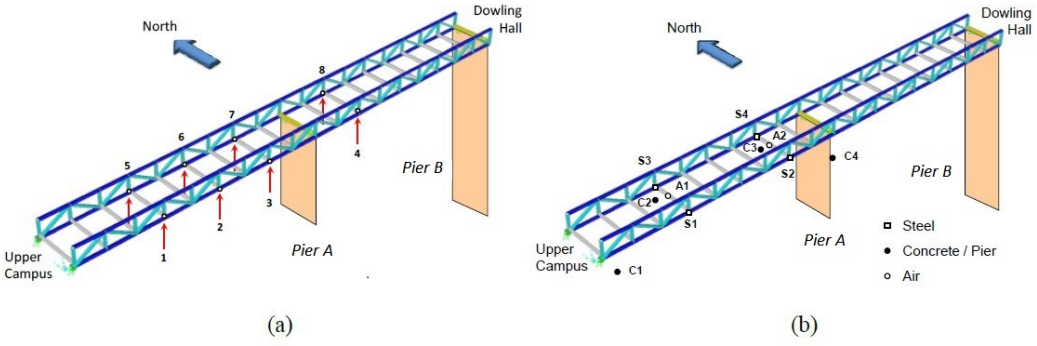

Figure 1.3 Locations of (a) accelerometers, and (b) thermocouples on Dowling Hall Footbridge (Moaveni and Behmanesh 2012)

In 2013, four accelerometers and four strain gauges were positioned on the bridge in addition to the already existing sensors, as displayed in Figure 1.4. The current continuous monitoring system is equipped with twelve accelerometers and four strain gauges that measure ambient acceleration and strain response of the bridge to wind and/or pedestrian traffic, as well as ten thermocouples to monitor temperature of the air, steel frame, concrete deck and piers.

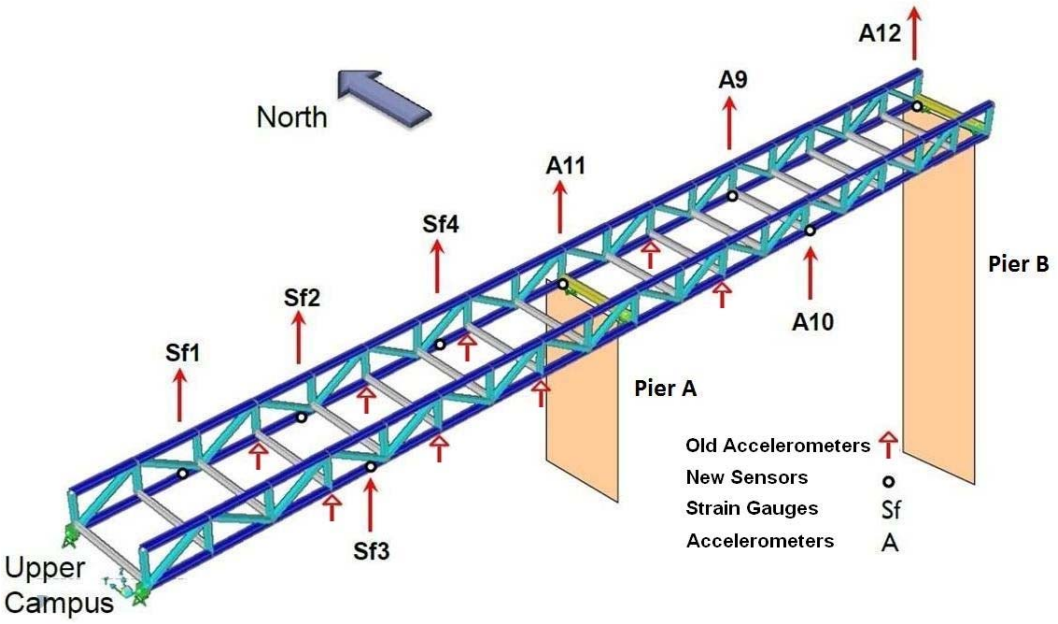

Figure 1.4 Locations of newly installed sensors on Dowling Hall Footbridge

The type of all twelve acceleration sensors is PCB Piezoelectronics model 393B04 accelerometer while the type of strain gauges is PCB Piezoelectronics model 740B02 strain sensor. It is expected that the piezo-electric strain sensors have less sensitivity to temperature than traditional foil strain gauges. The temperature range of the accelerometers is 0 to +176 °F and temperature range of the strain gauge is -65 to +250 °F. Absolute values of sensor measurements

depend on the temperature but the dynamic response should not be affected much by temperature changes. The accelerometers were installed at the underside of the stringer to girder connections. The strain gauges were attached on the bottom surface of girder members (Figure 1.5). All the waterproof sensors were connected by cables to a data acquisition device installed in an enclosure located on the abutment on the campus-side. The acceleration and strain channels are sampled continuously at a rate of 2048 Hz. Recording of a five-minute data set is automatically triggered every thirty minutes, at the beginning and in the middle of the hour, or when the one-second root-mean square (RMS) value of any acceleration channel exceeds 0.03g. More information about the continuous monitoring system can be found in Moser and Moaveni (2013).

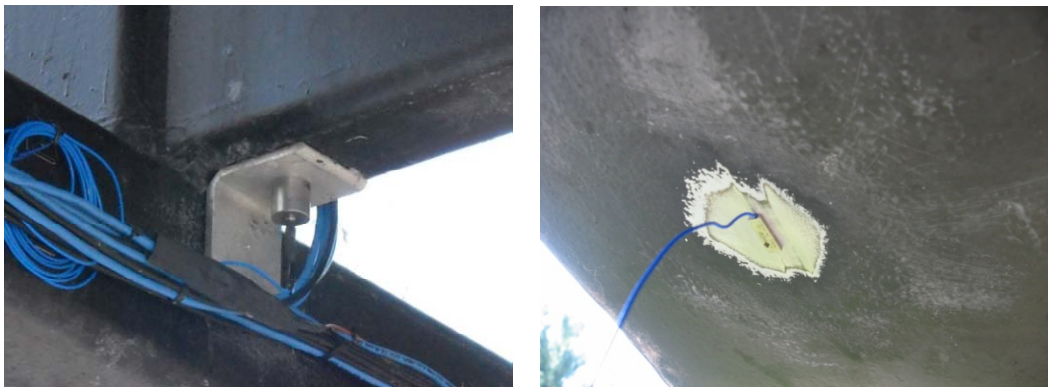

(a) (b)

Figure 1.5 (a) Accelerometers and (b) strain gauges

An automated operational modal analysis is performed based on each data set to extract the bridge's modal parameters (natural frequencies, mode shapes and strain mode shapes). Modal analysis process is based on an output-only stochastic subspace identification method (SSI) using filtered and down-sampled ambient vibration data (Van Overschee and De Moor 1996, Peeters and De Roeck 1999).

Natural frequencies and mode shapes of the 1st six vibration modes of the footbridge were identified from a preliminary test on April 4, 2009, as shown in Figure 1.6. Details about data cleaning process and modal analysis are also available in Moser and Moaveni (2013).

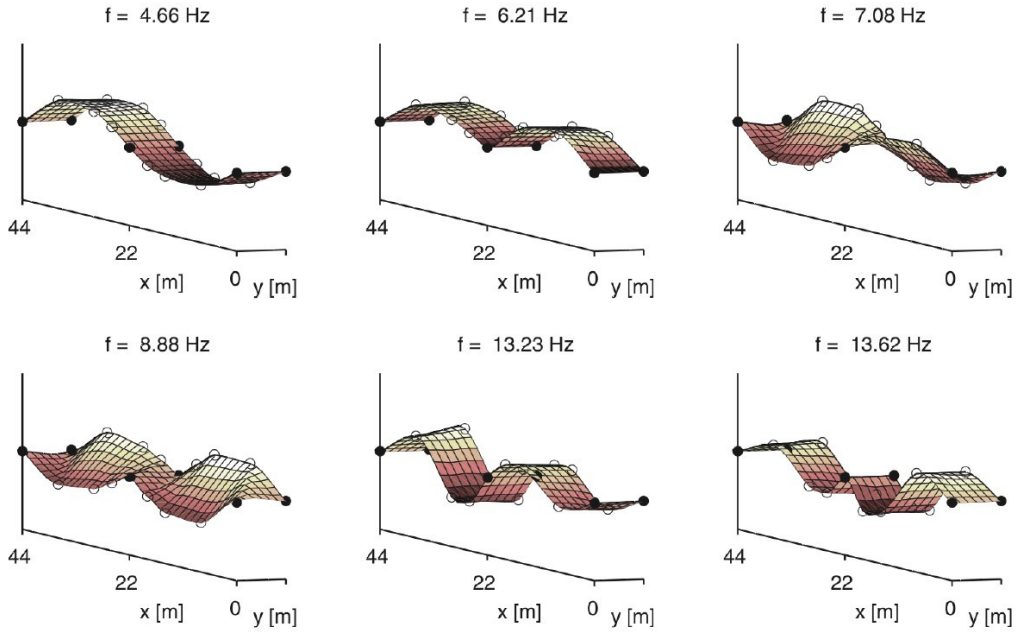

Figure 1.6 Modal parameters of the footbridge (Moser and Moaveni 2013)

1.4 Focus of Research

In this thesis, a model-based damage identification method, based on natural frequencies, mode shapes and strain mode shapes, is presented. The method is applied to estimate damage of the Dowling Hall footbridge, on which non-destructive damage is simulated in the form of concrete blocks loaded on the deck. A reference finite element (FE) model of the footbridge was calibrated so that it could simulate the physical behavior of the undamaged structure. Using a

sensitivity-based FE model updating method, this model was updated to reflect the "damaged" structure by minimizing the differences between experimental and analytical modal data. Finally the damage pattern was obtained from the comparison between the updated model with the reference model.

Furthermore, the effects of number, locations and types of sensors on performance of damage identification are investigated. Three cases of FE model updating were performed using: (1) measurements from eight accelerometers, (2) measurements from twelve accelerometers, and (3) measurements from twelve accelerometers and four strain gages. In the first step of this study, the reference FE model was updated using numerically simulated "damaged" modal data generated by "damaged" FE model, in which the same amount of mass had been added on the same locations as the real structure. The statistical variability of the identified damage parameters was estimated in the presence of added noise. The three cases of FE model updating were also applied to the actually measured experimental data of the Dowling Hall Footbridge and the results of damage identification were compared with the exact values of damage (added mass). Finally, the statistics of the identified damage parameters from the numerical study were compared with those from the experimental work and accuracy of each case was analyzed individually.

1.5 Organization of Thesis

Chapter one provides background and motivation for structural health monitoring. Then a brief description of the Dowling Hall footbridge and the continuous

monitoring system is given. Finally, focus and outline of works in this study are clarified.

Chapter two mainly reviews the process of the deterministic finite element (FE) model updating method applied in this study. FE modeling of the footbridge, modal analysis of the model, formulation of objective function, and calculation of sensitivity matrix, are discussed.

Chapter three presents the damage identification study and obtained results. First, the loading plan of concrete blocks on the Dowling Hall footbridge as simulated damage is introduced. Then the studies of numerical and experimental FE model updating for damage identification are presented. Finally, the results from both numerical and experimental applications are discussed and conclusions are made.

Chapter four summarizes the conclusions of this study and provides some suggestions for future research.

Chapter 2 Finite Element Model Updating

2.1 Introduction

Finite element (FE) models are commonly used for analysis of structural and mechanical systems. Detailed FE models are becoming used more commonly for structure design and analysis in recent years, taking advantage of the tremendous developments in calculation capacity of computers. Thus, reliable predictions of dynamic structural behavior can be made if the FE model is an accurate representation of the real structure.

It is worth noting that effects of modeling errors always exist for real-world structures such as buildings and bridges. In creating FE models, engineering assumptions are made to simplify complex structures. Moreover, initial models are usually based on visual inspection and design drawings, which may be inaccurate. Therefore the initial FE model is not usually very accurate to represent the real structure. If measured data are available from the actual structure, effects of modeling errors can be minimized by calibrating the initial FE model to match the measured data.

Sensitivity-based FE model updating technique can be used for calibration of an initial FE model. This technique belongs to the class of inverse problems. Inverse problems typically refer to estimation of certain parameters in the FE model such as stiffness or mass based on measured data such as acceleration response or modal parameters (i.e., natural frequencies and mode shapes) extracted from

acceleration response. For example, in a forward problem dynamic characteristics are calculated directly by analysis of the FE model with known physical parameters, whereas in an inverse problem physical parameters are adjusted so that model-predicted response of the structure can match the measured values of dynamic response. Using measured vibration data such as acceleration and/or strain, FE model updating can provide structure's physical parameters, such as mass and stiffness, which are hard to measure directly. Consequently, FE model updating ensures that the updated model can fit the measured data and further confirm the consistency between FE model and the actual structure. FE model updating can also be used for damage identification. If two different FE models are fit to the data from the undamaged/baseline state and damaged state of a structure, then the change in the physical modeling parameters, such as stiffness, can be defined as damage. Overview of the sensitivity-based updating methods can be found in Link (1999).

In this chapter, theoretical background of the FE model updating is presented. The initial FE model of the Dowling Hall footbridge is discussed. The procedure to form the modal residuals and the considered objective functions are explained. The analytical sensitivities of the residuals with respect to the updating parameters are derived. Finally, the information gained about the updating parameters from the measured data is quantified.

2.2 Initial FE Model of the Dowling Hall Footbridge

An initial finite element model of the Dowling Hall footbridge was created based on the design drawing of the bridge, which can be found in Bowman (2003). The structural analysis software FEDEASLab (Filippou and Constantinides, 2004) was adopted to build up the initial FE model of the Dowling Hall footbridge (Moaveni and Behmanesh, 2012). FEDEASLab is structural analysis software programmed in Matlab. The introduction and several simulation examples of FEDEASLab are available in Filippou and Constantinides (2004).

A three-dimensional rendering of the FE model (created in SAP2000) is demonstrated in Figure 2.1. The model consists of 356 elements and 197 nodes, with each element comprising two or four nodes. Following assumptions are made to develop the initial model: (1) the element connections are all rigid; (2) the three supports (pier A, pier B and the abutment) are modeled as springs; (3) masses of the concrete deck and railings are assigned at the nodes of finite element; (4) every node has six degrees of freedom, three are translational and the other three are rotational, whereas only the vertical translational DOF's assumed to have non-zero mass and the horizontal translational DOF's have zero mass. The rotational DOF's are also assumed to have zero-mass moment of inertia. This assumption is based on the fact that only vertical accelerations are measured on the Dowling Hall Footbridge, and the ambient responses of the bridge in the horizontal directions are relatively small. Therefore, the updating process mainly focuses on the vertical dynamic motion of the structure and its FE model. The

zero-mass DOF's are condensed at the stiffness matrix before performing eigen-analysis. These assumptions have simplified the complicated structure and reduced the computation time needed for dynamic analysis without significant compromise in the accuracy of obtained modal parameters. After static condensation, the structural response at horizontal translational and rotational DOF's can be computed relative to the translational DOF's. Note that there are nodes in the model at the locations of accelerometers in the real structure.

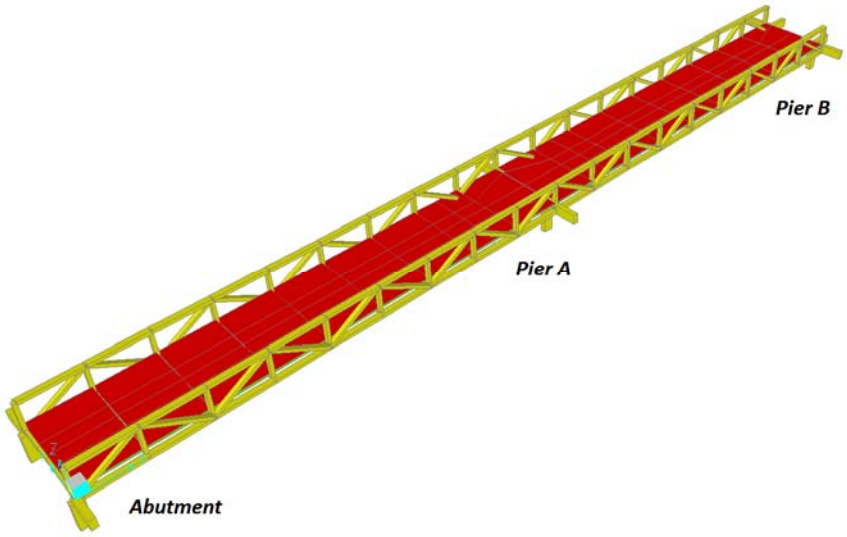

Figure 2.1 Finite element model of the Dowling Hall Footbridge
(Kody and Moaveni, 2011)

2.3 Modal Analysis of the FE Model

Despite possible existence of measurement errors, the experimental vibration data obtained from the test is considered to be a reliable representation of the structure behaviors. In this thesis, FE model updating procedure is performed by tuning the model parameters (stiffness or mass) so that the model's modal parameters match the experimental data. As mentioned in Section 1.3, the continuous monitoring

system installed on the Dowling Hall footbridge is equipped with an automated operational modal analysis framework. This system extracts modal parameters from experimental vibration data measured by the sensors every hour or every 30 minutes. The modal parameters include natural frequencies, mode shapes and strain mode shapes of the 1st six modes. On the other hand, the analytical modal parameters are derived from performing an eigen-analysis of the condensed stiffness and mass matrices obtained from the FE model.

2.3.1 *Natural Frequencies and Mode Shapes*

Finite element method (FEM) is performed to determine the natural frequencies and mode shapes of the FE model. The eigenvalues and eigenvectors obtained by solving the eigensystems can represent the natural frequencies and corresponding mode shapes. The dynamic equation of motion is given as:

$$[\mathbf{M}][\ddot{\mathbf{U}}]+[\mathbf{C}][\dot{\mathbf{U}}]+[\mathbf{K}][\mathbf{U}]=[\mathbf{F}] \tag{2.1}$$

where $[\mathbf{M}]$, $[\mathbf{C}]$ and $[\mathbf{K}]$ are the FE model's mass matrix, damping matrix and stiffness matrix, respectively. If the model has totally N degrees of freedom, $[\mathbf{M}]$, $[\mathbf{C}]$ and $[\mathbf{K}]$ are all N by N square matrices. $[\mathbf{F}]$ is the force vector and $[\mathbf{U}]$ represents the displacement of each degree of freedom. Dot above $\mathbf{U}$ means the time derivative, thus $[\dot{\mathbf{U}}]$ is the velocity and $[\ddot{\mathbf{U}}]$ is the acceleration. For modal analysis, the damping matrix is generally ignored, and force vector is assumed zero, then equation (2.1) can be written as:

$$[\mathbf{M}][\ddot{\mathbf{U}}]+[\mathbf{K}][\mathbf{U}]=[\mathbf{0}] \tag{2.2}$$

By solving eigenvalue problem associated with equation (2.2) based on known **[M]** and **[K]**, eigenvalues and eigenvectors can be calculated, which reflect the square of circular natural frequencies and corresponding mode shapes of the model. As mentioned in Section 2.2, the rotational DOF's are assigned zero mass moment of inertia. Thus, the partitioned form of equation (2.2) is:

$$\begin{bmatrix} \mathbf{m}_{tt} & \mathbf{0} \\ \mathbf{0} & \mathbf{0} \end{bmatrix} \begin{bmatrix} \ddot{\mathbf{u}}_t \\ \ddot{\mathbf{u}}_r \end{bmatrix} + \begin{bmatrix} \mathbf{k}_{tt} & \mathbf{k}_{tr} \\ \mathbf{k}_{rt} & \mathbf{k}_{rr} \end{bmatrix} \begin{bmatrix} \mathbf{u}_t \\ \mathbf{u}_r \end{bmatrix} = \begin{bmatrix} \mathbf{0} \\ \mathbf{0} \end{bmatrix} \tag{2.3}$$

where the subscript t stands for translational and r means rotational. Solving equation (2.3) leads to:

$$\mathbf{u}_r = -\mathbf{k}_{rr}^{-1}\mathbf{k}_{rt}\mathbf{u}_t \tag{2.4}$$

which confirms the assumption that the rotational DOF's $\mathbf{u}_r$ are determined by the translational DOF's $\mathbf{u}_t$. Notes that as the horizontal translational DOF's also own zero mass, $\mathbf{u}_r$ contains not only rotational DOF's but also DOF's in two horizontal translational directions, which are also totally dependent on $\mathbf{u}_t$ including vertical DOF's with non-zero mass. Next, substituting equation (2.4) in equation (2.3) gives:

$$\mathbf{m}_{tt}\ddot{\mathbf{u}}_t + \hat{\mathbf{k}}_{tt}\mathbf{u}_t = \mathbf{0} \tag{2.5}$$

in which

$$\hat{\mathbf{k}}_{tt} = \mathbf{k}_{tt} - \mathbf{k}_{rt}^{T}\mathbf{k}_{rr}^{-1}\mathbf{k}_{rt} \tag{2.6}$$

The hat on top means it is the condensed stiffness matrix. The matrix eigenvalue problem of equation (2.5) is:

$$\left[\hat{\mathbf{k}}_{tt} - \omega_n^2 \mathbf{m}_{tt}\right]\boldsymbol{\Phi}_n^{(t)} = \mathbf{0}, \quad n = 1,....,N_t \tag{2.7}$$

N_t denotes the number of free translational DOF's that have non-zero mass in the FE model. ω_n is the n^{th} natural frequencies and $\boldsymbol{\Phi}_n^{(t)}$ contains the mode shape components of the translational DOF's. The rotational mode shape components can be obtained using equation (2.4):

$$\boldsymbol{\Phi}_n^{(r)} = -\mathbf{k}_{rr}^{-1}\mathbf{k}_{rt}\boldsymbol{\Phi}_n^{(t)}, \quad n = 1,....,N_t \tag{2.8}$$

Equation 2.8 provides the relationship between condensed and full DOF mode shapes. The full mode shapes consist of both translational and rotational components:

$$\boldsymbol{\Phi}_n = \begin{bmatrix} \boldsymbol{\Phi}_n^{(t)} \\ \boldsymbol{\Phi}_n^{(r)} \end{bmatrix}, \; n = 1,....,N_t \tag{2.9}$$

Considering the fact that data collected from the continuous monitoring system provides certain components of vertical mode shapes, the numerical mode shapes used for model updating should include only the same measured DOF's. The full (translational and rotational) mode shapes will be used to find out numerical strain mode shapes later. The 1^{st} six vibration modes obtained from modal analysis of this FE model is demonstrated in Figure 2.2.

Only mode shapes components corresponding to DOF's measured on the real structure were used in the FE model updating. These DOF's corresponded to the 12 acceleration measurements on the bridge.

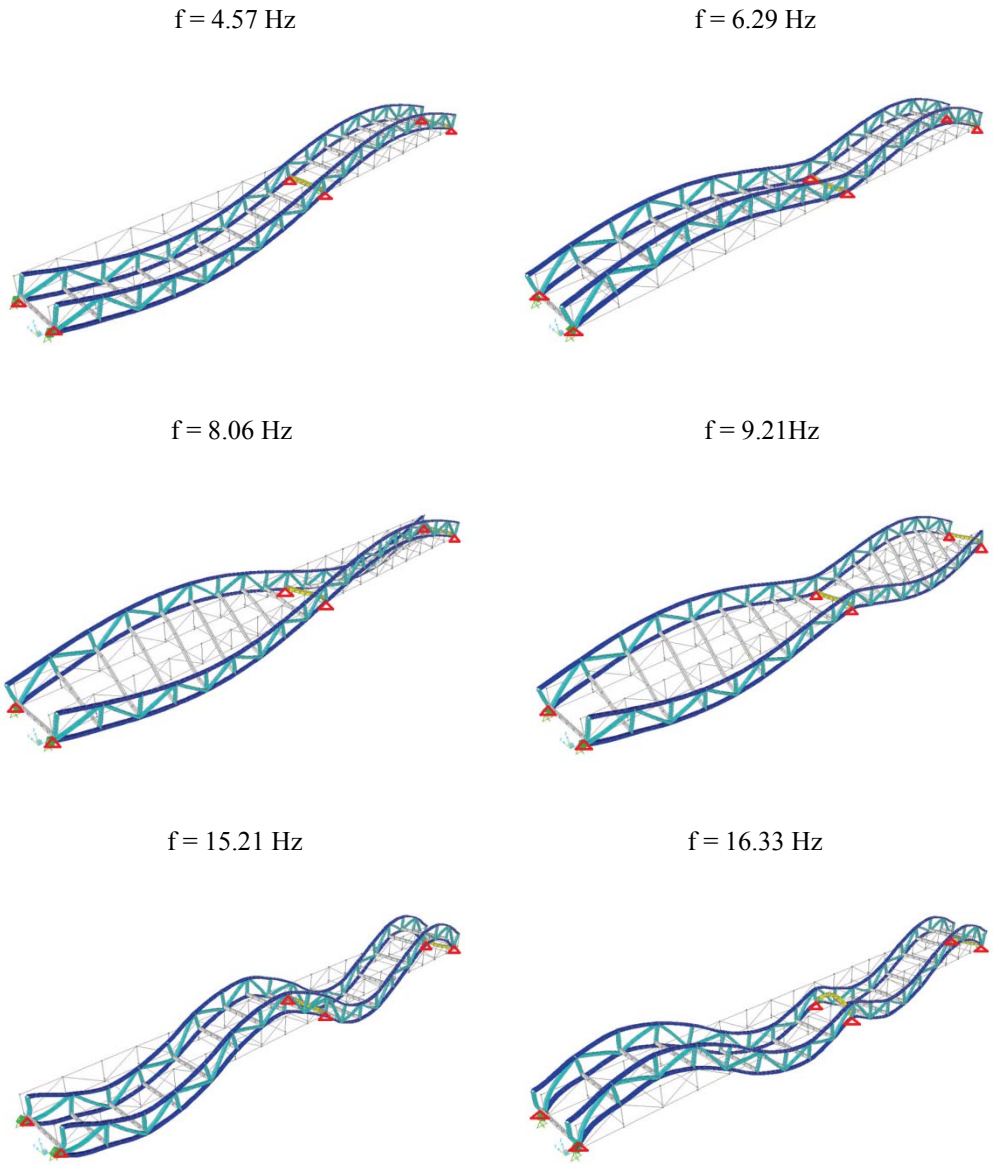

Figure 2.2 Vibration modes of Dowling Hall Footbridge from computer modeling (Moser and Moaveni, 2013)

2.3.2 *Strain Mode Shapes*

In addition to the natural frequencies and (displacement) mode shapes, model updating is also performed using strain mode shapes. The experimental strain mode shapes were extracted from data measured by four strain gauges on the bridge. Strain gauge measures the local dynamic deformation or the local strain on element where the strain gauge is located. The numerical strain mode shapes can be obtained by calculation of strains on the four elements where strain gauges are attached.

The change in length of the strain gauge can be computed from its nodal displacements (Conte and Liu 2000). Figure 2.3 shows the 2D geometric parameters of one element with strain sensor on it. The strain sensor is commonly attached to the surface of the element parallel to its neutral axis. $u_1^{(i)}$ to $u_6^{(i)}$ are the local nodal displacements of the element *i*.

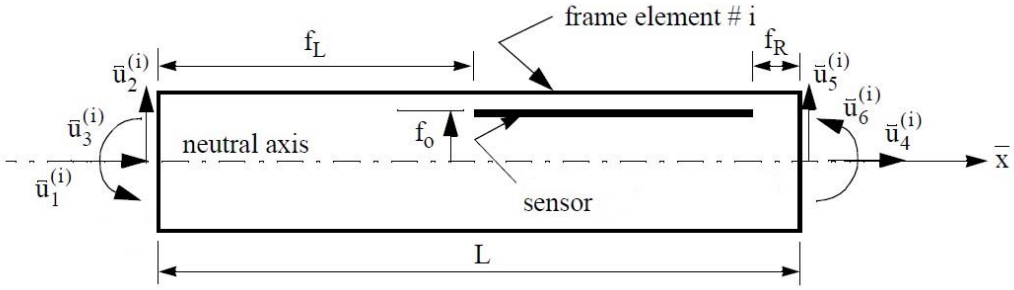

Figure 2.3 Embedded strain sensors in a single frame element
(Conte and Liu, 2000)

f_L = distance from left end of strain sensor to left end of the element.
f_R = distance from right end of strain sensor to right end of the element.
f_o = vertical distance from strain sensor to neutral axis.

As discussed in Conte and Liu (2000), the length change of the partial element overlapped by the sensor can be calculated by integrating the axial strain $\varepsilon_{\bar{x}\bar{x}}$, along the length of the element $\bar{x}$:

$$\Delta_f = \int_{f_L}^{L-f_R} \varepsilon_{\bar{x}\bar{x}} \, d\bar{x} = \int_{f_L}^{L-f_R} \left(\bar{u}'_{axial} - f_0 \cdot \bar{u}''_{transverse} \right) d\bar{x} \tag{2.10}$$

Therefore the equation to calculate the measured deformation Δ_f is:

$$\Delta_f = \bar{u}_{axial} \Big|_{f_L}^{L-f_R} - f_0 \cdot \bar{u}'_{transverse} \Big|_{f_L}^{L-f_R} \tag{2.11}$$

In equation (2.11), $\bar{u}_{axial}$ is the axial displacement field and $\bar{u}_{transverse}$ is the transverse displacement field along axis of element *i*. Both of them are functions with respect to $\bar{x}$. $\bar{u}_{axial}$ and $\bar{u}_{transverse}$ are calculated as: (2.10)

$$\begin{aligned} \bar{u}_{axial}(\bar{x}) &= (\bar{u}_4 - \bar{u}_1)/L \\ \bar{u}_{transverse}(\bar{x}) &= \sum_{j=2,3,5,6} \bar{u}_j \cdot \beta_j(\bar{x}) \end{aligned} \tag{2.12}$$

In equation (2.12), $u_2^{(i)}$ and $u_5^{(i)}$ are the vertical translational components, $u_1^{(i)}$ and $u_4^{(i)}$ are the axial translational components, while $u_3^{(i)}$ and $u_6^{(i)}$ are the rotational components of the mode shapes that are related to DOF's of the two nodes composing this element. β_j is defined by the following equations.

$$\begin{aligned} \beta_2(\bar{x}) &= 1 - 3\left(\frac{\bar{x}}{L}\right)^2 + 2\left(\frac{\bar{x}}{L}\right)^3 & \beta_3(\bar{x}) &= \bar{x}\left(1 - \frac{\bar{x}}{L}\right)^2 \\ \beta_5(\bar{x}) &= 3\left(\frac{\bar{x}}{L}\right)^2 - 2\left(\frac{\bar{x}}{L}\right)^3 & \beta_6(\bar{x}) &= \frac{\bar{x}^2}{L}\left(\frac{\bar{x}}{L} - 1\right) \end{aligned} \tag{2.13}$$

β_j is only dependent on location of strain gauge, therefore the numerical strain is purely a function of the full mode shape corresponding to the nodal DOF's of the element. The equation for strain mode shapes can be written as:

$$\Phi_{st}^{(i)} = \mathbf{T}_{\mathrm{f}}^{(i)} \cdot \boldsymbol{\Phi}^{(i)} \tag{2.14}$$

where $\Phi_{st}^{(i)}$ is one of the strain mode shape components (scalar) along the strain gauge on element *i*. $\boldsymbol{\Phi}^{(i)}$ is mode shape vector containing translational and rotational DOF components of element *i*, $u_1^{(i)}$ to $u_6^{(i)}$. $\mathbf{T}_{\mathrm{f}}^{(i)}$ is the transformation matrix derived from equations (2.12) and (2.13).

Locations of the four strain gauges on the Dowling Hall footbridge are shown in Figure 1.4. The length of each strain gauge is 0.6 inch (15.2 mm). Figure 2.4 presents location of one of these strain gauges along the girder.

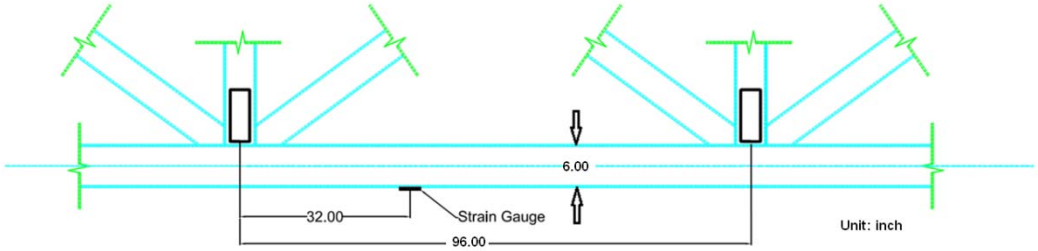

Figure 2.4 Configuration of one of the strain gauges on the Dowling Hall footbridge

The sensor is installed on the bottom of the girder. For this element, f_o = 3 in, f_L = 31.7 in, f_L = 63.7 in and L = 96 in. The numerical strain on this point can therefore be calculated based on equation (2.14), in which $\mathbf{T}_{\mathrm{f}}^{(i)}$ is:

$$\mathbf{T}_{\mathrm{f}}^{(i)} = \left[-\frac{1}{L} \quad -f_0\left(\frac{12\bar{x}}{L^2} - \frac{6}{L^2}\right) \quad -f_0\left(\frac{6\bar{x}}{L^2} - \frac{4}{L}\right) \quad \frac{1}{L} \quad f_0\left(\frac{12\bar{x}}{L^2} - \frac{6}{L^2}\right) \quad -f_0\left(\frac{6\bar{x}}{L^2} - \frac{2}{L}\right) \right]_{f_L}^{L-f_R} \tag{2.15}$$

Similarly, strains on the other three points equipped with strain gauges are also obtained and together four strains form the strain mode shapes.

2.4 Objective Function

The FE model updating is performed through minimizing an objective function or cost function. The objective function is defined as a sum of squared differences (or residuals) between measurements from actual structure and those from the FE model (Teughels, 2003).

Objective function contains the discrepancies between analytical data from FE model, which depend on the parameters to be updated, and experimental vibration data obtained from real structure. By adjusting the updating (physical) parameters of FE model, objective function is minimized and therefore the FE model can better reflect the actual building. Finding parameters that minimize the objective function is equivalent to solving a nonlinear least squares problem (Friswell and Mottershead, 1995). Sensitivity-based optimization methods are commonly used to find the optimum solution. The iterative optimization procedure is performed by solving a least squares problem, which is an efficient approach and has been commonly used to solve the updating problem. In FE model updating, the objective function $f(\boldsymbol{\theta})$ can be written as:

$$f(\boldsymbol{\theta}) = \frac{1}{2}\mathbf{r}(\boldsymbol{\theta})^T \boldsymbol{W}\, \mathbf{r}(\boldsymbol{\theta}) \tag{2.16}$$

where $\boldsymbol{W}$ is the weighting matrix, which will be discussed in Section 2.4.4, $\boldsymbol{\theta}$ includes the updating parameters, $\mathbf{r}$ is the residual vector, expressing the

difference between experimentally identified modal parameters and their analytical counterparts numerically obtained using FE model. Size of **r** depends on the sizes of experimental modal parameters, namely, the number of sensors in the monitoring system and number of modes extracted through modal analysis. Residual vector **r** consists of natural frequency or eigenfrequency residuals $\mathbf{r}_f$, mode shape residuals $\mathbf{r}_s$ and strain mode shape residuals $\mathbf{r}_{st}$. Definition of each residual will be discussed later. The residual vector **r** is shown below:

$$\mathbf{r}(\boldsymbol{\theta}) = \begin{bmatrix} \mathbf{r}_f(\boldsymbol{\theta}) \\ \mathbf{r}_s(\boldsymbol{\theta}) \\ \mathbf{r}_{st}(\boldsymbol{\theta}) \end{bmatrix} \tag{2.17}$$

Before comparing the identified modal data and the FE computed values, they must be paired to represent the same mode. Because in practical experiment, only a few of the excited lower vibration modes can be identified accurately, whereas a significantly large number of analytical modes can be captured from the FE model. Although arranging eigenfrequencies in ascending order helps for pairing, order of modes close to each other may be reversed, which is called mode crossing phenomenon. Due to modeling errors and/or inaccurate measurements, the orders of modes in numerical model and experimental data can differ. The most common and effective way for mode matching, is to pair the modes with largest modal assurance criterion (MAC) values (Allemang and Brown, 1982):

$$MAC\left(\boldsymbol{\Phi}_i, \tilde{\boldsymbol{\Phi}}_j\right) = \frac{\left|\boldsymbol{\Phi}_i^T \tilde{\boldsymbol{\Phi}}_j\right|^2}{\left(\boldsymbol{\Phi}_i^T \boldsymbol{\Phi}_i\right)\left(\tilde{\boldsymbol{\Phi}}_j^T \tilde{\boldsymbol{\Phi}}_j\right)} \tag{2.18}$$

where $\boldsymbol{\Phi}$ can be recognized as mode shape or strain mode shape vector. i and j are the number of corresponding modes. The superposed tilde refers to experimental data. A MAC value is always between 0 and 1. MAC value equal to 1.0 means the two modes are 100% matching and value of zero denotes that no correlation can be found (i.e. modes are orthogonal). For one experimental mode shape, MAC values of this mode shape with all the available analytical mode shapes are calculated using equation (2.18), and the one that shows the highest value is picked as its analytical counterpart for updating. In this way, correlations between experimental and analytical modal parameters are established before formulating the residual functions.

2.4.1 *Eigenfrequency Residuals*

The first residual contains the discrepancies between analytical and experimental eigenfrequencies. The eigenvalue λ, which is the square of the circular natural frequency, is used in formulation of this residual:

$$r_f^i(\boldsymbol{\theta}) = \frac{\lambda_i(\boldsymbol{\theta}) - \tilde{\lambda}_i}{\tilde{\lambda}_i}, \qquad i = 1,....,m_f \tag{2.19}$$

with eigenvalue $\lambda_i = (2\pi f_i)^2$ and natural frequencies f_i. m_f refers to the number of identified modes that are used in the updating process. λ_i and $\tilde{\lambda}_i$ denote the numerical and corresponding experimental eigenvalue, respectively. $\boldsymbol{\theta}$ is the vector of updating parameters. Compared with the other residuals, eigenfrequency residuals are usually assigned larger weights because eigenfrequency is usually identified more accurately and has higher sensitivity to the structure's physical

properties, especially mass and stiffness. Therefore eigenfrequency residuals make the most significant contribution to the FE model updating.

2.4.2 *Mode Shape Residuals*

Even though the eigenfrequencies are sensitive to mass and stiffness of the structure, they provide only global information about these physical parameters**.** To be able to localize the change in mass and stiffness, spatial information with respect to the dynamic behavior of the structure is needed. Thus, residuals of mode shape are formulated to represent the modal displacement of the structure as complements to eigenfrequency residuals. The mode shape residuals are defined as:

$$\boldsymbol{r}_s^i(\boldsymbol{\theta}) = \frac{\boldsymbol{\Phi}_i^l(\boldsymbol{\theta})}{\Phi_i^r(\boldsymbol{\theta})} - \frac{\tilde{\boldsymbol{\Phi}}_i^l}{\tilde{\Phi}_i^r}, \qquad i = 1, ..., m_s \tag{2.20}$$

where $\boldsymbol{\Phi}_i$ and $\tilde{\boldsymbol{\Phi}}_i$ are the analytical and corresponding experimental mode shapes of vibration mode i. m_s is the number of identified mode shapes taken into consideration in the updating process. The superscript r indicates the reference DOF, and superscript l refers to the other measured DOF's except the reference. Since mode shapes extracted from experimental data and those identified using FE model are not scaled similarly, normalization process is necessary before comparison. Usually the reference DOF is selected as the DOF with the largest absolute value of mode shape component, so different vibration modes have different reference DOF's. Both analytical and identified mode shapes are normalized with respect to the same reference channel to be comparable. The amplitude of this reference DOF is normalized to unit 1 and other components of

the mode shape are normalized by being divided by the value of reference amplitude. Note that the FE model computed mode shapes have a large number of DOF's, while only modal displacements of nodes that are measured should be selected for the updating (i.e., nodes at the locations of sensors).

The mode shape residuals are providing information about the location of changes between model and data. However, in order to have spatially refined model updating, a large number of sensors are necessary to cover the overall structure. This limitation makes it difficult to update too many parameters especially for a large structure. Moreover, mode shapes cannot be identified as easily and accurately as eigenfrequencies and mode shape residuals are less sensitive to mass and stiffness parameters compared with eigenfrequency residuals. Therefore the weights of mode shape residuals in model updating should be no heavier than natural frequencies. Despite all the disadvantages, the utility of mode shapes is still essential in the FE model updating procedure considering the extra information they offer. It is worth mentioning that the accelerometers working on the Dowling Hall footbridge measure only vertical acceleration.

2.4.3 *Strain Mode Shape Residuals*

In this study, the effects of using strain mode shapes in FE model updating are also studied. Strain at any point of the structure can be measured directly using strain sensors attached on or embedded in that point. Strain mode shapes are computed through modal analysis of measurements from strain sensors. Similar to the mode shape residual, strain mode shape residual can be written as:

$$\boldsymbol{r}_{st}^{i}(\boldsymbol{\theta}) = \frac{\boldsymbol{\Phi}_{st,i}^{l}(\boldsymbol{\theta})}{\Phi_{st,i}^{r}(\boldsymbol{\theta})} - \frac{\tilde{\boldsymbol{\Phi}}_{st,i}^{l}}{\tilde{\Phi}_{st,i}^{r}}, \qquad i = 1,....,m_{st} \tag{2.21}$$

in which $\boldsymbol{\Phi}_{st,i}$ and $\tilde{\boldsymbol{\Phi}}_{st,i}$ are the analytical and corresponding experimental strain mode shapes of vibration mode *i,* respectively. m_{st} is the number of identified strain mode shapes considered in the updating process. The superscript *r* and *l* indicates the reference strain, and other strains used in the model updating. The process of normalization and pairing for strain mode shapes are similar to those of mode shapes. Four strain gauges are installed on the Dowling Hall footbridge measuring the ambient vibration strain response of the structure at four points.

In addition to the information about displacement mode shape inferred by accelerometers, strain measurements provide complementary spatial information about updating parameters. Strain-measurements are especially sensitive to local changes, i.e., provide accurate estimation of an updating parameter at the location of sensor. However, this sensitivity decreases fast the further away from the location of the strain sensor. Thus, approximated location of expected change should be known before installing the strain sensors. Furthermore, disadvantages of mode shapes stated before are also shared by strain mode shapes. Actually, more strain gauges are needed than accelerometers in order to successfully detect global damage in a structure. In this study, the contribution of the strain mode shape to FE model updating and damage identification is investigated.

2.4.4 *Weighting Matrix*

$\boldsymbol{W}$ in equation (2.16) is the residual weighting matrix. Values of weights in this diagonal matrix are determined based on the estimated reliabilities of the experimental modal parameters, ranging from 0 to 1.0. Inaccuracies caused by noise or estimation errors are inevitable in both measurement and modal identification procedures. The larger the error, the less reliable the corresponding residual is in the updating and therefore the weight assigned to this residual should be smaller. For example, eigenfrequencies are identified with higher accuracy than the mode shapes, thus have larger weight. The relative weighting matrix controls the weights of different types of residuals, as well as weights of different modes within one type of residual. It allows the residuals to be weighted individually based on their uncertainty and importance, where the latter one can be quantified by sensitivity test.

2.5 Updating Factors

2.5.1 *Model Parameters to be Updated*

There are a large number of parameters in the FE model, such as material properties, geometric properties and boundary conditions. However, not all the parameters need to be updated because some parameters have already been accurately estimated, such as the geometric properties. In the application of FE model updating for damage identification, damage is usually indicated in the form of stiffness reduction. Thus, stiffness of selected elements in the FE model is usually updated for damage identification. Mass matrix of the model can also be

included in model updating if it is expected that there is large uncertainty in estimated mass of the structure. However, usually both the mass and stiffness matrices are not updated simultaneously due to compensation effects.

In this study, three types of modal parameter residuals (natural frequency, mode shape and strain mode shape) are used for model updating. For one mode, each type of residual is given the same total weight, i.e., sum of weighs for mode shape residuals of mode one is equal to sum of the weights of strain mode shape residuals of that mode before taking into account the influence of sensor errors. For example, if 12 accelerometers and 4 strain gauges are used to measure data and provide corresponding modal parameters, the residual with respect to one mode will contain 15 components: one eigenfrequency residual, eleven mode shape residuals (one component is selected as reference), and three strain mode shape residuals. Therefore, the weights given to each component will be w_i for frequency, $w_i / 11$ for mode shape and $w_i / 3$ for strain mode shape. The weights w_i for different modal frequencies will be further adjusted based on the identification accuracy of each mode in the experimentally measured modal data.

2.5.2 *Substructuring*

Even when the updating parameters are limited to stiffness or mass, their number can still be very large, for example 356 for individual element stiffness or 197 for nodal mass. The limited amount of information in the measured data makes it difficult/impossible to update all of these parameters due to ill-conditioning of the problem. Thus, it is not possible to update all the mass or stiffness variables

simultaneously as individual components. In this study, substructuring is applied as a mean to reduce the number of updating parameters by dividing the FE model into several segments and grouping the properties of elements/nodes in each segment together. As demonstrated in Figure 2.5, FE model of the footbridge is divided into 6 substructures (or segments) based on the locations of accelerometers.

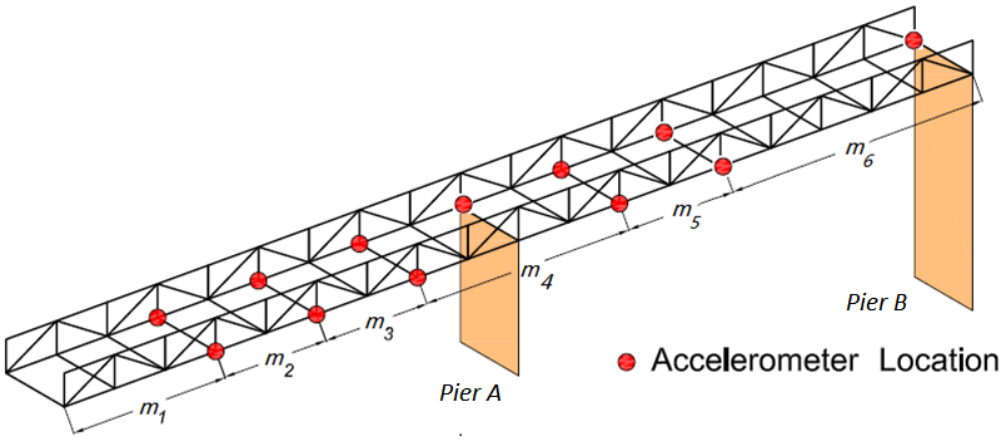

Figure 2.5 Updating substructures of footbridge (Moser and Moaveni 2013)

Therefore, only 6 parameters in the FE model are tuned in the process of FE model updating. Each substructure is composed of all the elements and nodes that are located in the corresponding segment of the bridge. A damage function is used to correlate the updated value of the stiffness (or mass) at different elements (or nodes) in a substructure with the single substructure updating factor. The substructure updating factors are damage factor $\boldsymbol{a}$ for stiffness updating and added mass $\Delta\boldsymbol{m}$ for mass updating, both of which are vectors containing six updating factors for the six substructures. The damage functions' sizes are 356 by

6 for the case of updating stiffness (bridge has 356 elements) or 197 by 6 for the case of updating mass (bridge has 197 nodes).

2.5.3 *Updating Stiffness*

If there is no prior knowledge about the distribution of damage within one substructure, the proportional loss of stiffness seems the most reasonable assumption. However, if a specific distribution of damage is available based on prior knowledge, damage in individual elements may be assigned using a given pattern. Such pattern is implemented when updating the mass and is based on the tributary area of nodes. In this study, damage factor $\boldsymbol{a}$ is implemented for stiffness updating and is defined as reduction ratio of the effective modulus of elasticity:

$$a^{\mathrm{e}} = \frac{E^{\mathrm{e}}_{\mathrm{undamaged}} - E^{\mathrm{e}}_{\mathrm{damaged}}}{E^{\mathrm{e}}_{\mathrm{undamaged}}} \tag{2.22}$$

where E^{e} is the effective Young's modulus of elasticity of an element in substructure e. The correction values are considered to be constant for all elements belonging to the same substructure. Therefore, components of damage function related to updated elements in the same substructure are uniform and all have the value of 1.0. It means that for each element, its EA, EI, and GJ are changing proportionally. For the damage function with full size of 356 by 6, if the element i belongs to the segment j, the value of component in the location of i and j of the damage function matrix is 1.0, otherwise it is zero. In this approach, damage factor $\boldsymbol{a}$, containing a_1 to a_6, are capable of reflecting stiffness varieties

of all the elements in the FE model. The range of damage factors are restricted to [-0.99, 0.99] during calibration of the initial model to gain the reference model presenting the actual undamaged structure.

2.5.4 *Updating Mass*

Although damage of the structure usually refers to reduction in the stiffness of structure members and connections, equation (2.2) shows that adding mass to the model can affect the modal data in a similar way as reducing the stiffness. Thus, updating the mass is alternatively a reasonable route for model calibration. The correction factor $\Delta \boldsymbol{m}$ is composed of values of masses added on the substructures.

$$\Delta m^{\mathrm{n}} = m^{\mathrm{n}}_{\mathrm{damaged}} - m^{\mathrm{n}}_{\mathrm{undamaged}} \tag{2.23}$$

with m^{n} is the lumped mass at node n. Unlike the damage factor $\boldsymbol{a}$, the damage function of $\Delta \boldsymbol{m}$ is not uniform along one substructure and the values for different nodes depend on contributing area of deck. $\Delta \boldsymbol{m}$ is made up of Δm_1 to Δm_6, corresponding to total value of added mass on different substructures. The total added mass in one substructure is not distributed uniformly. For example, if the added mass is loaded on a segment of the bridge's deck, nodes at edges of the segment will have less added mass than the nodes in the middle (different tributary area). Careful consideration is needed to determine the damage function values for added mass in different nodes of a substructure.

2.6 Sensitivity Matrix

To solve the nonlinear least squares problem as a sensitivity-based procedure, an iterative optimization method is used based on the sensitivity of residuals to the updating parameters in the FE model. Thus, calculation of the Jacobian matrix (or the sensitivity matrix) is essential within the iterative optimization process. The Jacobian matrix contains the first-order partial derivatives of residuals r (eigenfrequency, mode shape and strain mode shape residual) with respect to the updating parameter θ (mass or stiffness of the FE model):

$$\boldsymbol{J}_{\boldsymbol{\theta}} = \begin{bmatrix} \frac{\partial r_1}{\partial \theta_1} & \cdots & \frac{\partial r_1}{\partial \theta_n} \\ \vdots & \ddots & \vdots \\ \frac{\partial r_m}{\partial \theta_1} & \cdots & \frac{\partial r_m}{\partial \theta_n} \end{bmatrix}_{mxn} \tag{2.24}$$

where m is the number of residuals in the objective function and n is the number of physical parameters to be adjusted in the FE model. In order to calculate $\boldsymbol{J}$, the derivatives of modal parameters with respect to the updating parameters need to be calculated first. The method provided by Fox and Kapoor (1968) to calculate these derivatives is based on the equation (2.2) and specific derivation process of the following two equations is available in Appendix C of Teughels (2003). The equation to obtain sensitivity of eigenvalue λ_j is:

$$\frac{\partial \lambda_j}{\partial \theta^e} = \boldsymbol{\Phi}_j^T \left[\frac{\partial \boldsymbol{K}}{\partial \theta^e} - \lambda_j \frac{\partial \boldsymbol{M}}{\partial \theta^e} \right] \boldsymbol{\Phi}_j \tag{2.25}$$

and sensitivity of corresponding mode shape $\boldsymbol{\Phi}_j$ is given by:

$$\frac{\partial \boldsymbol{\Phi}_j}{\partial \theta^e} = \sum_{q=1;q\neq j}^{d} \left(\frac{\boldsymbol{\Phi}_q}{\lambda_j - \lambda_q} \boldsymbol{\Phi}_q^T \left[\frac{\partial \boldsymbol{K}}{\partial \theta^e} - \lambda_j \frac{\partial \boldsymbol{M}}{\partial \theta^e} \right] \boldsymbol{\Phi}_j \right) - \frac{\boldsymbol{\Phi}_j}{2} \boldsymbol{\Phi}_j^T \frac{\partial \boldsymbol{M}}{\partial \theta^e} \boldsymbol{\Phi}_j \qquad (2.26)$$

For both equations, θ denotes the updated values of mass or stiffness in the FE model. The stiffness matrix $\boldsymbol{K}$ and mass matrix $\boldsymbol{M}$ of the model are respectively functions of element stiffness k^e and node mass m^n. Thus, if the unknown parameter is stiffness, $\partial \boldsymbol{M} / \partial \theta^e$ becomes zero; on the contrary, $\partial \boldsymbol{K} / \partial \theta^e$ will be canceled if θ refers to mass. The sensitivity of strain mode shapes can be derived from the sensitivity of mode shapes on the basis of equation (2.14):

$$\frac{\partial \boldsymbol{\Phi}_{st,j}^{(i)}}{\partial \theta} = \mathbf{T}_{\mathrm{f}}^{(i)} \cdot \frac{\partial \boldsymbol{\Phi}_j^{(i)}}{\partial \theta} \qquad (2.27)$$

Substituting equations (2.25), (2.26) and (2.27) in residual equations (2.19), (2.20) and (2.21) gives formulas for sensitivities of residuals r_f, r_s and r_{st}:

$$\frac{\partial r_f}{\partial \theta} = \frac{1}{\tilde{\lambda}_j} \frac{\partial \lambda_j}{\partial \theta} \qquad (2.28)$$

$$\frac{\partial r_s}{\partial \theta} = \frac{1}{\boldsymbol{\Phi}_j^r} \frac{\partial \boldsymbol{\Phi}_j^l}{\partial \theta} - \frac{\boldsymbol{\Phi}_j^l}{\left(\boldsymbol{\Phi}_j^r\right)^2} \frac{\partial \boldsymbol{\Phi}_j^r}{\partial \theta} \qquad (2.29)$$

$$\frac{\partial r_{st}}{\partial \theta} = \frac{1}{\boldsymbol{\Phi}_{st,j}^r} \frac{\partial \boldsymbol{\Phi}_{st,j}^l}{\partial \theta} - \frac{\boldsymbol{\Phi}_{st,j}^l}{\left(\boldsymbol{\Phi}_{st,j}^r\right)^2} \frac{\partial \boldsymbol{\Phi}_{st,j}^r}{\partial \theta} \qquad (2.30)$$

which will together formulate the Jacobian matrix $\boldsymbol{J}_{\boldsymbol{\theta}}$. Because damage function is decided independently of $\boldsymbol{\theta}$, multiplying $\boldsymbol{J}_{\boldsymbol{\theta}}$ by different damage functions can offer Jacobian matrices with respect to substructure updating factors ($\boldsymbol{J}_{\boldsymbol{\alpha}}$ for stiffness damage factor and $\boldsymbol{J}_{\Delta \boldsymbol{m}}$ for added mass). The computed analytical

Jacobian matrix will be used in the FE model updating to find out the corresponding updating factors.

2.7 Information Gain in Model Updating

This section is focuses on estimation of information gain about the updating parameters when using the FE model updating process. Due to different sources or error, the estimated updating parameters are always uncertain. However, their degree of uncertainty depends on the available type, amount and accuracy of data. The accuracy of identified parameters are usually quantified by their bias (mean values) and standard deviation (Std) or coefficient of variance (COV). These values can be computed by repeating the identification/updating process when a large number of data sets are available. However, when measured data is not available, the information gain from potential residuals can be estimated by computing the Fisher Information Matrix and information entropy estimate.

The information entropy is defined in the context of *information theory*. It is usually used to quantify the uncertainty in random variables and the value of information contained in a set of data. The information entropy is often applied to the Bayesian model updating method to determine the uncertainty of identified results. Generally, the smaller the value of information entropy relative to an event is, the less uncertainty it will contain. In this study, the information entropy is based on the Fisher Information matrix (FIM) from the sensitivity matrix $\boldsymbol{J}_{\boldsymbol{\theta}}$. It means that the information entropy is correlated to the sensitivity of residuals to

the updating parameters and has the capability to measure the uncertainty in the calibrated FE model. The information entropy can be estimated as:

$$h(\boldsymbol{\theta}) \approx \frac{1}{2} N \log(2\pi e) - \frac{1}{2} \log\left[\det \boldsymbol{Q}(\boldsymbol{\theta})\right] \tag{2.31}$$

where $\boldsymbol{Q}$ stands for the FIM, with regards to the identified parameters θ. FIM contains information about values of parameters in θ based on measured data used in FE model updating. FIM varies with the locations and number of sensors used in the monitoring system (Papadimitriou 2004). In this research, FIM is used to calculate the information entropy and uncertainty of updating parameters obtained when using different number and type of sensors. Since only the uncertainty in model updating is considered in this study, only the 2nd term in equation (2.31) is considered here:

$$h(\boldsymbol{\theta}) \approx -\frac{1}{2} \log\left[\det \boldsymbol{Q}(\boldsymbol{\theta})\right] \tag{2.32}$$

The FIM is equal to the Hessian matrix of the objective function that can be estimated as $\boldsymbol{Q}(\boldsymbol{\theta}) \approx \boldsymbol{J}_{\boldsymbol{\theta}}^{T} \boldsymbol{W} \boldsymbol{J}_{\boldsymbol{\theta}}$, where $\boldsymbol{W}$ denotes the weighting matrix and its components are normalized in the range between 0 and 1.0. Then equation (2.32) can be simplified to:

$$h(\boldsymbol{\theta}) \approx -\frac{1}{2} \sum_{k=1}^{N_p} \log \lambda_k \tag{2.33}$$

with λ denotes the eigenvalues of the Hessian matrix $\boldsymbol{Q}$. N_p is the number of updating parameters as well as the size of $\boldsymbol{Q}$. By computing $h(\boldsymbol{\theta})$ for different

types of residuals, the added information and uncertainty contained in the corresponding calibrated model can be quantified. Further assessment on influence of different data set can be performed that allows evaluating the effects of number and types of sensors on the accuracy of damage identification results.

2.8 Conclusion

This chapter introduces the theoretical background of FE model updating and the specific details used in the application of FE model updating for damage identification of Dowling Hall Footbridge. This method is capable of three levels of damage identification, namely detection, localization and quantification of the damage, which can refer to changes in stiffness and/or mass of a structure. The first step in application of FE model updating for damage identification is to create an undamaged or reference model to be compared with the "damaged" actual structure. Since the physical parameters of the structure such as stiffness and/or mass cannot be measured directly, modal parameters of the structure are extracted from ambient vibration data measured by accelerometers and strain gauges. By minimizing the difference between experimental and numerical modal parameters, the reference model is calibrated to reflect the actual structure and the damage can be localized and quantified. Finally, statistical data and information entropy corresponding to estimated FE parameters from each data set can be calculated to analyze the influence of number and types of sensors on accuracy of damage identification results.

Chapter 3 Damage Identification

3.1 Introduction

In this Chapter, the FE model updating technique is applied for damage identification of the Dowling Hall footbridge using numerically simulated and experimentally measured data. Although loss of stiffness is the most common damage in structures, it is not possible to physically simulate this type of damage on an in-service footbridge with frequent passage of pedestrians. Also, for the purpose of evaluating the performance of FE model updating for damage identification, it is desirable that the extent of induced damage can be exactly known. Therefore, instead of reducing the stiffness of the Dowling Hall Footbridge, damage in this study was simulated on the bridge by addition of mass. Addition of mass has similar effects on the modal parameters of a structure as the loss of stiffness.

FE model updating has been previously applied by several researchers for model calibration and/or damage identification of civil structures. Friswell and Mottershead (1995) describe the FE model updating method and the optimization problem related to the objective function formed by different residuals. Doebling et al. (1996, 1998) provide a comprehensive review of vibration-based damage identification methods including FE model updating. In Zhang et al. (2000, 2001), FE model updating is performed to detect the health conditions of structural connections and boundary conditions of the Kap Shui Mun cable-stayed bridge by

minimizing the difference in natural frequencies. Since natural frequencies alone are generally not adequate to localize the damage, mode shapes are usually used in FE model updating as it is done by Moaveni et al. (2008) for damage identification of a full-scale composite beam. Sanayei and Saletnik (1996) use direct strain measurements in FE model updating for structural parameters identification. Brownjohn et al. (2003) quantify the effectiveness of refurbishing works on a highway bridge in Singapore through FE model updating with data before and after the strengthening of the bridge. Moaveni and Behmanesh (2012) give insight into the ambient temperature effects on FE model updating results by adjusting the Young's modulus of members of the Dowling Hall footbridge at different ambient temperatures. In this study, performance of FE model updating is investigated when applied for identification of simulated damage on the Dowling Hall Footbridge using its continuously measured ambient vibration response. Variability in the estimated damage identification results as well as effectiveness of the measured data for calibrating selected model parameters is discussed.

3.2 Damage Simulation

As previously discussed, damage on the Dowling Hall Footbridge was simulated by increasing the mass of bridge deck. To achieve this, concrete blocks were placed on the sides of the deck along different segments of the bridge. The concrete blocks, shown in Figure 3.1, are $8\text{in}\times 4\text{in}\times 16\text{in}$ in size and weight 33.1 lbs. when dry and 34.3 lbs. when wet. The cubic shape guarantees that blocks can

keep tight to each other when stacked together, such that the added mass can be considered as uniformly distributed on the loading area.

Figure 3.1 The loading concrete block

Prior to moving blocks on the bridge, long wood boards were put on the surface of loading area to protect the deck. Loading has been confirmed to cause no actual damage to the members and connections of the bridge (Kody and Moaveni, 2011) and the loading experiment had been authorized by Tufts University. The blocks were delivered to the deck of the bridge by carts and placed in the loading area. After the stacking work finished, a plastic construction mesh was covered on the blocks and fixed by tape. Subsequently caution signs were also deployed to warn the pedestrians.

The loading test was performed in three phases. In the first phase, 2,247 kg (150 x 33 lbs concrete blocks totaling 4950 lbs) was placed within substructure 2 as shown in Figure 3.3. During the second phase, 1,348 kg (90 x 33 lbs concrete blocks totaling 2970 lbs) was placed within substructure 2 and an additional 1,348 kg placed on the Dowling Hall side of the bridge in a symmetric loading (Figure 3.4). In the third phase, 1,348 kg (150 x 33 lbs concrete blocks totaling 2970 lbs) remained on the Dowling Hall side of the bridge as shown in Figure 3.5. An analysis in SAP2000 structural analysis software was performed before the test to

determine the approximate percent reduction in natural frequencies due to the addition of mass on the deck. Based on these analyses and the knowledge from the previous tests, the locations and magnitude of the added mass was determined for the loading test.

The blocks were moved onto the bridge at 3:20 pm, May 31, 2013 and taken away at 4 pm, June 10, 2013. The overall effective loading period was from 4:30 pm, May 31 to 3:30 pm, June 10, 2013. The overall periods of three phases are shown in Table 3.1:

Table 3.1 Loading plan

	Period	Loading Condition	
		Substructure 2	Substructure 5
Phase 1	05/31, 16:30 ～ 06/03, 17:30	150 blocks, 4950 lbs.	0
Phase 2	06/03, 18:00 ～ 06/06, 17:00	90 blocks, 2970 lbs.	90 blocks, 2970 lbs.
Phase 3	06/06, 17:30 ～ 06/10, 15:30	0	90 blocks, 2970 lbs.

In Phase 1, a total of 150 blocked were used. 75 blocks were stacked on each side of the deck on substructure 2, with 3 rows high and 25 blocks in each row. In Phase 2, 90 blocks were loaded on both substructure 2 and substructure 5. The stacking patterns were the same for each substructure: 23 blocks on the bottom row and 22 blocks on the top row on each side. In Phase 3, the 90 blocks on substructure 5 remained in place while the blocks on substructure 2 were removed. It took less than 30 minutes to position the blocks and safety measures between each phase so the time history of measured data was continuous. After the loading experiment ended, all the blocks and safety measures were removed and the bridge deck was cleaned.

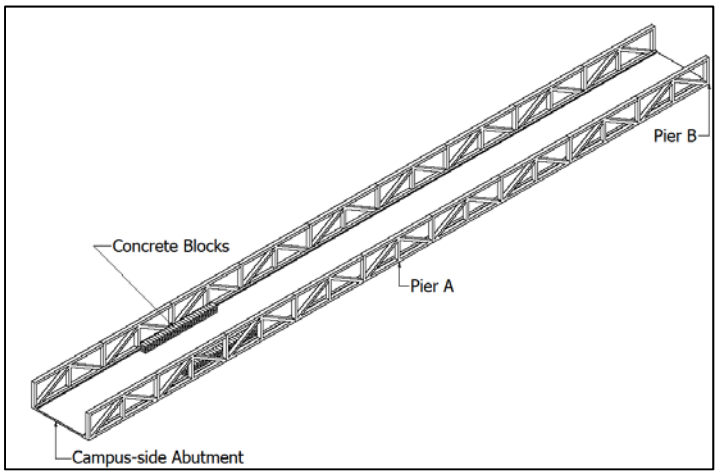

Figure 3.2 Loading plan: Phase 1 (substructure 2) (Kody, 2013)

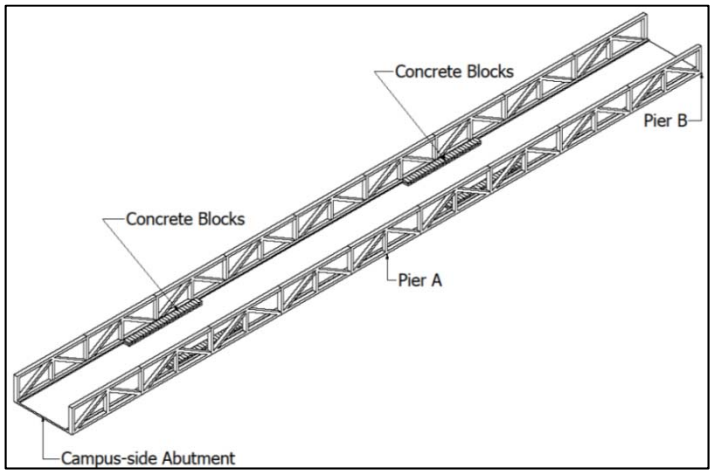

Figure 3.3 Loading plan: Phase 2 (substructure 2 and 5) (Kody, 2013)

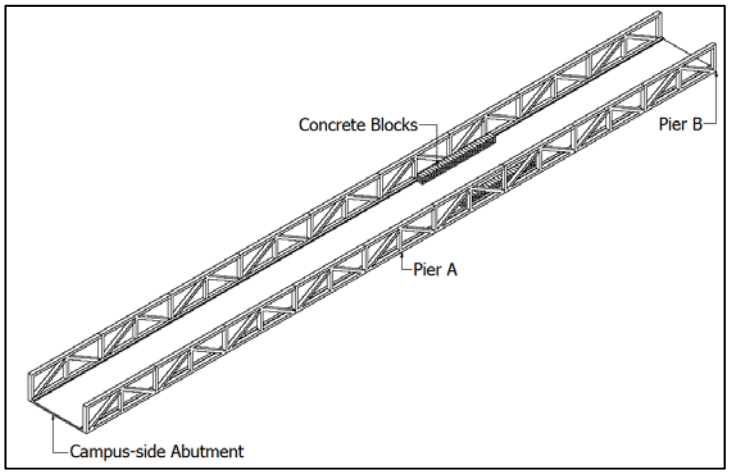

Figure 3.4 Loading plan: Phase 3 (substructure 5) (Kody, 2013)

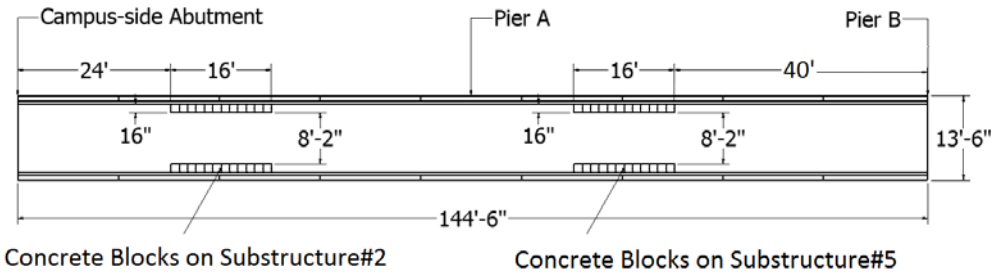

Figure 3.5 Deployment of concrete blocks on the bridge (Kody, 2013)

(a) (b)

Figure 3.6 Blocks stack in (a) Phase 1, and (b) Phase 2

3.3 System Identification

The continuous monitoring system installed on the bridge records five minutes of ambient vibration data every 30 minutes, so 147 data sets were recorded in Phase 1, 143 data sets in Phase 2 and 189 data sets in Phase 3. Automatic system identification is used to extract the modal parameters (natural frequencies, mode shapes and strain mode shapes) of the bridge from each data set (Moser, 2010). In this study, the 1st six modes identified from acceleration data and the 1st four modes identified using strain measurements are used for the damage identification. These modes are the most excited vibration modes and thus, are more reliably identified compared to the higher modes. However, because of the measurement noise and identification errors, not all the six modes can be

identified accurately from each data set. Thus, an initial analysis had been done to determine the reliability and accuracy of the identified modal parameters of these six vibration modes. Table 3.2 presents the identification success rate of each mode during this experiment. A vibration mode is successfully identified when it is found to be stable for five consecutive model orders. At a certain model order, a mode is stable when it satisfies the following three conditions (1) its natural frequency is within 0.01 of the mean natural frequencies for all previous orders, (2) its mode shape has a MAC value of higher than 95% with the average mode shape, and (3) damping ratio is within 0.3% of average damping ratio. More details can be found in Moser and Moaveni (2013).

Table 3.2 Identification success rate

	Mode 1	Mode 2	Mode 3	Mode 4	Mode 5	Mode 6
Phase 1	91%	34%	99%	100%	95%	96%
Phase 2	90%	30%	99%	100%	96%	92%
Phase 3	84%	19%	100%	100%	96%	96%
Total Period	88%	27%	100%	100%	96%	95%

It demonstrates the success rate in percentage for different modes and different tests. It can be seen that mode 2 is poorly identified in all three phases with an overall 27% identification success rate. On the contrary, modes 3 and 4 are almost always identified. Modes 5 and 6 are identified around 95% of the time while mode 1 has a relatively lower rate of under 90%, which are regarded as a reasonably good identification rate. It can be concluded that the weight of mode 2 applied in FE model updating should be much smaller than the other modes because the 2nd mode is hardly identified. However, it should be noted that having

a higher identification success rate does not necessarily mean that a mode is identified accurately as its estimation error may be large. Despite the high rate of identification rate of the other five modes, their weights in the FE model updating were not equal. Other factors are considered in order to evaluate the accuracy of identified modal parameters.

In Figure 3.7, the identified natural frequencies before and after the loading tests are plotted. The "undamaged" natural frequencies are obtained using the data measured from 5 pm, May 28 to 4 pm, May 31 of 2013, right before the loading tests. This data contains 112 sets of modal parameters. The last set corresponds to 4 pm, May 31 and was taken during the loading process. It is not accurate and should be neglected.

A distinguished decrease in the identified natural frequencies of modes 1, 3 and 4 can be observed when the loading begins. Mode 5 does not show a clear reduction as the other modes, but it is the only mode that presents relatively evident differences between Phase 1 and Phase 2. The decreasing trend caused by loading cannot be observed apparently in mode 2 and mode 6. In conclusion, the plots reveal that: (1) mode 1, 3 and 4 are highly qualified for damage identification because of their high identification success rates and high sensitivities to change of mass; (2) modes 5 and 6 are not as sensitive to the added mass as the previous three modes, although they have high identification success rate; (3) mode 2 is poorly identified so it should not be included for the damage identification. Therefore, modal parameters of mode 1, 3 and 4 were considered as the most accurately identified parameters and larger weight were assigned to their

corresponding residuals in the objective function. Specific analysis to determine the weighting matrix will be given in Section 3.5.

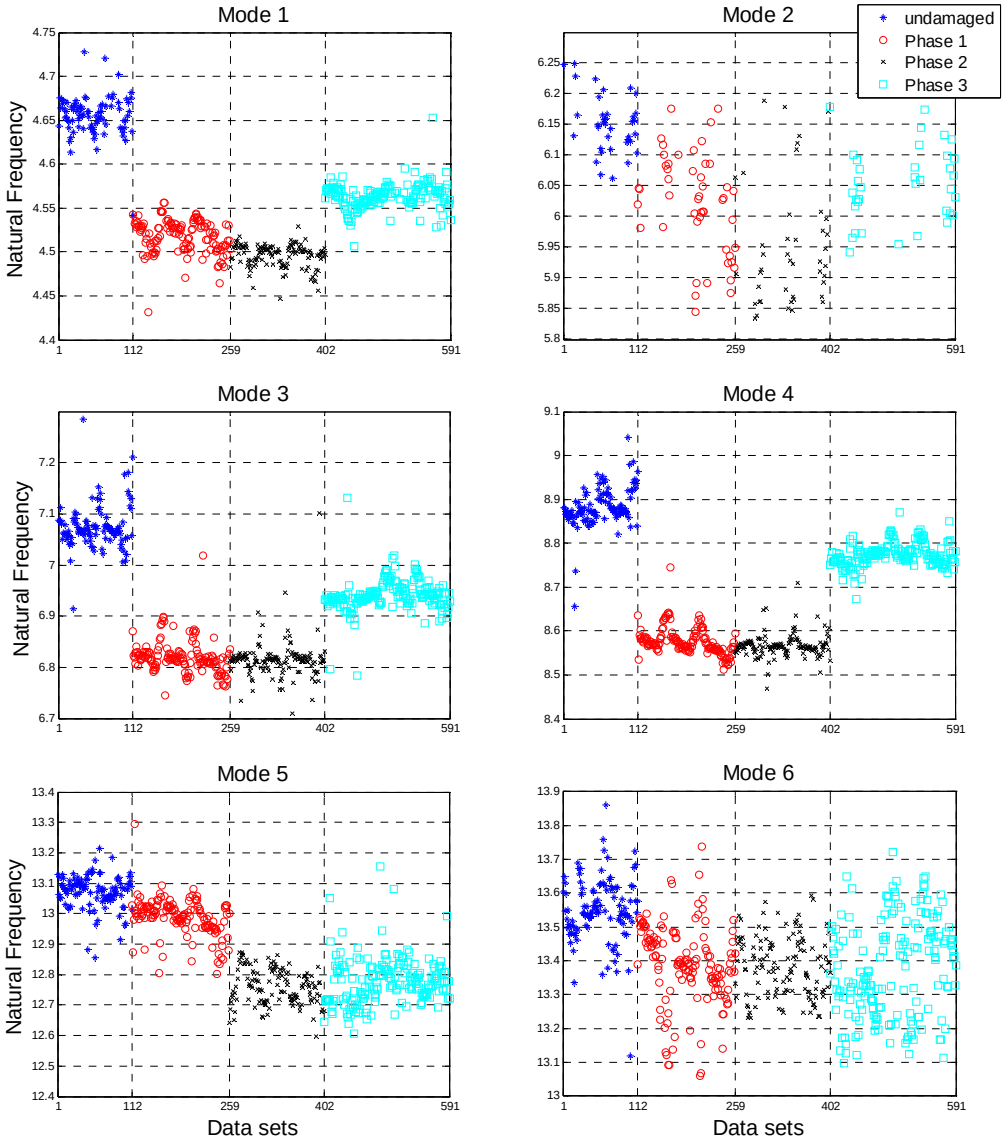

Figure 3.7 Natural frequencies extracted by identification (unit: Hz)

3.4 Damage Identification Using Numerical Data

Before the sensitivity-based FE model updating was used for damage identification based on the experimentally identified modal parameters obtained from "damaged" bridge, performance of this method was systematically studied

when damaged data were simulated using the FE model of the bridge. It is performed to validate the implementation and assess the accuracy of this method under known level of error in modal parameters and no modeling errors in the FE model. To simulate the data for damaged structure, the same quantities of masses as in the loading tests are added numerically on the initial FE model of the bridge and the modal parameters at the locations of sensors are extracted. The modal parameters are then polluted with zero-mean Gaussian white noise to represent the "noise-polluted" data. Finally, these polluted sets of modal parameters are used as "experimental" data sets in the FE model updating, and the values of updating results are compared with the exact values of added mass on the FE model. Through this simulation, FE model updating is tested under the condition of no modeling error but in the presence of specific estimation errors due to noise and environmental variability.

3.4.1 *Numerical Damage Scenarios*

The numerical damage scenarios considered here are identical to the damage simulated on the footbridge as explained in Section 3.2, i.e., there are three phases of loading and the masses are added only on substructure 2 and substructure 5: (1) 4.95 kips added on substructure 2; (2) 2.97 kips added on each of substructures 2 and 5, and (3) 2.97 kips added on substructure 5.

In the FE model, all the masses are assigned at the element nodes. Because the concrete blocks are loaded on the deck of bridge, only nodes that constitute the deck are considered to be affected by the added mass. Uniform distribution of the

mass requires every node to have its own factor depending on the corresponding tributary area. If one node is located at the edge of the loading area, the factor assigned is equal to 0.5. Similarly, nodes at corners of loading area will have factors equal to 0.25 and nodes located in the center will have factors of 1.0. For example, as shown in Figure 3.8, 4 kips mass is loaded on the shadowed area consisting of nodes A - I. Nodes A - D will have factors of 0.25, nodes E - H will have factors of 0.5, and node I will have a factor of 1.0. Added mass on nodes with factor = 1.0 can be calculated as Δm = 4 ÷ (¼ · 4 + ½ · 4 + 1.0) = 1 kips for node I. Nodes A - D would have ¼ Δm = 0.25 kips and nodes E - H have ½ Δm = 0.5 kips added.

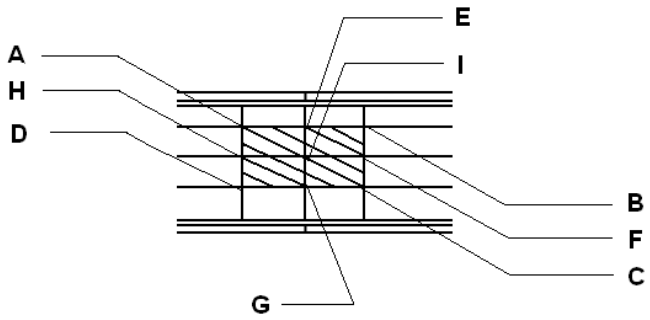

Figure 3.8 Example of loading mass on FE model

The initial FE model was created as discussed in Section 2.2 based on the design drawings. According to previously discussed loading plans, three "damaged" FE models were generated corresponding to the structures in the three phases of loading tests. Modal analysis is performed to extract modal parameters of the 1st six vibration modes including the natural frequencies, mode shapes and strain mode shapes at the location of sensors.

3.4.2 *Added Noise*

In order to investigate the effects of estimation errors in the identified modal parameters due to measurement noise, modal identification uncertainty, changing environmental effects and others, 100 vectors of zero-mean Gaussian white noises were created and added to the exacted modal parameters. Next, 100 sets of FE model updating were performed using the 100 sets of noisy modal parameters for each loading phase. The noise realizations were independent for the 100 sets and for the different modes and modal parameters. In order to generate the noise-polluted modal data, first a noise vector is realized (including 100 samples) randomly for each of the modal parameters. Then, the 100 components are normalized to have a zero mean and considered COV values. Finally, the noise vectors are added to the exact values of model parameters providing 100 sets of noisy modal data. After contamination, the mean value of each modal parameter component over the 100 sets is equal to the exact value of the modal parameter (zero bias). The coefficient of variation (COV) for each mode of the modal parameters is defined as reported in Table 3.3.

Table 3.3 COV of each mode (%)

	Mode 1	Mode 2	Mode 3	Mode 4	Mode 5	Mode 6
Natural Frequency	0.31	0.47	0.40	0.21	0.43	0.61
Mode Shape	0.31	0.47	0.40	0.21	0.43	0.61
Accurate Strain Mode Shape	(0.31/5)	(0.47/5)	(0.40/5)	(0.21/5)		
Inaccurate Strain Mode Shape	(0.31×5)	(0.47×5)	(0.40×5)	(0.21×5)		

After contamination, the mean value of each modal parameter over the 100 sets is equal to the exact value of the modal parameter (zero bias). The COV value of a random variable is defined as the ratio of the standard deviation to the mean, which is a normalized measure of dispersion of the identified parameter distribution. The COV values of natural frequencies are selected based on the statistics of modal parameters identified from measured data on the Dowling footbridge during 17 weeks (Moaveni and Behmanesh 2012). The mode shape of each mode is assumed to own same variability as the natural frequency of the corresponding mode and assigned the same COV value. In order to particularly investigate the contribution of strain sensors to providing useful information, the strain mode shapes were assigned two different COV values in two separate cases of model updating. In the first case, the COV values of strain mode shapes were set as 20% of those related to natural frequencies to simulate the situation that the strain sensors were more reliable than accelerometers, and inversely, in the second case, strain sensors were assumed to be less dependable and the COV values were defined as 5 times of those related to natural frequencies. Eventually, three groups of noise-polluted "damaged" modal parameters were designed. Each group referred to one loading phase and was formed of 100 sets of parameters, simulated based on the statistics of actual measured data. These data groups were used as numerically simulated "damaged" modal parameters in the FE model updating.

3.4.3 *FE Model Updating Results*

For each of the three considered loading phases, four cases of FE model updating were performed using modal parameters from: (1) 8 accelerometers, (2) 12 accelerometers; (3) 12 accelerometers plus 4 accurate strain gauges (strain mode shapes are more accurate than displacement modal shapes); and (4) 12 accelerometers plus 4 inaccurate strain gauges (strain mode shapes are less accurate than displacement modal shapes). The weight for each modal parameter residual in the objective function was assigned as the squared inverse of COV for that modal parameter. The following figures and tables display the results of damage identification as added mass on six substructures and their statistics. The tables contain the mean and standard deviation over 100 model updating runs in each of the four cases for Phases 1, 2 and 3, respectively. Note that the results in Tables 3.4 to 3.6 are obtained when the updating parameters (added mass on each substructure) were bounded between -5 and 7 kips. Figures 3.9 to 3.11 give the scatter of 100 identification results, exhibiting the variability of identification results. The solid line in each plot marks the exact value of added mass. Another set of FE model updating of the 1st three cases are performed for the three phases of damage when the updating parameters are constrained between 0 and 7 kips. The lower bound of zero can be justified by the fact that a reduction in the mass due to damage is not expected, which is similar to the assumption that an increase in stiffness of a structure due to damage is not expected. The statistics of the updating results with zero lower bounds are reported in Tables 3.7 to 3.9.

Table 3.4 Statistics of identified damage in Phase 1 (numerical)

Phase 1		Δm_1	Δm_2	Δm_3	Δm_4	Δm_5	Δm_6
Exact (kips)		**0**	**4.95**	**0**	**0**	**0**	**0**
Mean (kips)	Case 1	0.0138	4.9555	-0.0177	0.0410	-0.0072	0.0025
	Case 2	0.0148	4.9543	-0.0145	0.0251	-0.0034	0.0014
	Case 3	0.0040	4.9508	-0.0029	0.0146	0.0022	-0.0015
	Case 4	0.0135	4.9535	-0.0123	0.0026	-0.0022	0.0007
Std (kips)	Case 1	0.1076	0.0845	0.2270	0.9161	0.2492	0.1796
	Case 2	0.1044	0.0888	0.2606	1.0333	0.3076	0.2081
	Case 3	0.0820	0.0647	0.1007	0.4827	0.1149	0.1269
	Case 4	0.1035	0.0857	0.2456	0.9738	0.2865	0.1949

Table 3.5 Statistics of identified damage in Phase 2 (numerical)

Phase 2		Δm_1	Δm_2	Δm_3	Δm_4	Δm_5	Δm_6
Exact (kips)		**0**	**2.97**	**0**	**0**	**2.97**	**0**
Mean (kips)	Case 1	0.0135	2.9907	-0.0443	0.0922	2.9294	0.0303
	Case 2	0.0130	2.9906	-0.0408	0.0702	2.9406	0.0221
	Case 3	0.0029	2.9778	-0.0118	0.0237	2.9650	0.0061
	Case 4	0.0106	2.9886	-0.0360	0.0636	2.9435	0.0206
Std (kips)	Case 1	0.1384	0.1058	0.2336	1.0536	0.3368	0.2414
	Case 2	0.1297	0.1096	0.2590	1.1408	0.3739	0.2523
	Case 3	0.0908	0.0754	0.0856	0.5436	0.1513	0.1467
	Case 4	0.1297	0.1090	0.2425	1.0724	0.3503	0.2385

Table 3.6 Statistics of identified damage in Phase 3 (numerical)

Phase 3		Δm_1	Δm_2	Δm_3	Δm_4	Δm_5	Δm_6
Exact (kips)		**0**	**0**	**0**	**0**	**2.970**	**0**
Mean (kips)	Case 1	0.0054	0.0308	-0.0530	0.0965	2.9249	0.0344
	Case 2	0.0043	0.0309	-0.0498	0.0760	2.9367	0.0253
	Case 3	0.0015	0.0102	-0.0138	0.0190	2.9677	0.0045
	Case 4	0.0027	0.0282	-0.0444	0.0679	2.9407	0.0230
Std (kips)	Case 1	0.1742	0.1366	0.2289	1.0673	0.3500	0.2491
	Case 2	0.1677	0.1458	0.2559	1.1191	0.3855	0.2571
	Case 3	0.1055	0.0816	0.0801	0.5192	0.1636	0.1554
	Case 4	0.1684	0.1468	0.2398	1.0442	0.3608	0.2431

Table 3.7 Statistics of identified damage in Phase 1 (zero lower bound)

Phase 1		Δm_1	Δm_2	Δm_3	Δm_4	Δm_5	Δm_6
Exact (kips)		**0**	**4.95**	**0**	**0**	**0**	**0**
Mean (kips)	Case 1	0.0158	4.9707	0.0621	0.2073	0.0732	0.0493
	Case 2	0.0164	4.9660	0.0596	0.2026	0.0649	0.0368
	Case 3	0.0060	4.9533	0.0105	0.0495	0.0097	0.0060
Std (kips)	Case 1	0.1081	0.0770	0.1908	0.7282	0.2096	0.1515
	Case 2	0.1074	0.0765	0.1901	0.7280	0.2053	0.1563
	Case 3	0.0829	0.0638	0.0937	0.4283	0.1090	0.1237

Table 3.8 Statistics of identified damage in Phase 2 (zero lower bound)

Phase 2		Δm_1	Δm_2	Δm_3	Δm_4	Δm_5	Δm_6
Exact (kips)		**0**	**2.97**	**0**	**0**	**2.97**	**0**
Mean (kips)	Case 1	0.0143	3.0037	0.0867	0.2708	2.8537	0.0824
	Case 2	0.0360	2.9231	0.0127	0.3117	2.8984	0.0776
	Case 3	0.0361	2.9470	0.0140	0.1900	2.9308	0.0601
Std (kips)	Case 1	0.1362	0.1070	0.1808	0.8083	0.2604	0.1949
	Case 2	0.0609	0.1066	0.0390	0.4743	0.1225	0.1040
	Case 3	0.0548	0.0855	0.0351	0.2873	0.0934	0.0922

Table 3.9 Statistics of identified damage in Phase 3 (zero lower bound)

Phase 3		Δm_1	Δm_2	Δm_3	Δm_4	Δm_5	Δm_6
Exact (kips)		**0**	**0**	**0**	**0**	**2.970**	**0**
Mean (kips)	Case 1	0.0019	0.0482	0.0969	0.2692	2.8481	0.0877
	Case 2	0.0297	0.0250	0.0084	0.2333	2.9207	0.0941
	Case 3	0.0343	0.0222	0.0121	0.1666	2.9334	0.0689
Std (kips)	Case 1	0.1790	0.1416	0.1792	0.7993	0.2750	0.2015
	Case 2	0.0653	0.0555	0.0337	0.3884	0.1962	0.1094
	Case 3	0.0598	0.0439	0.0339	0.2638	0.1019	0.0896

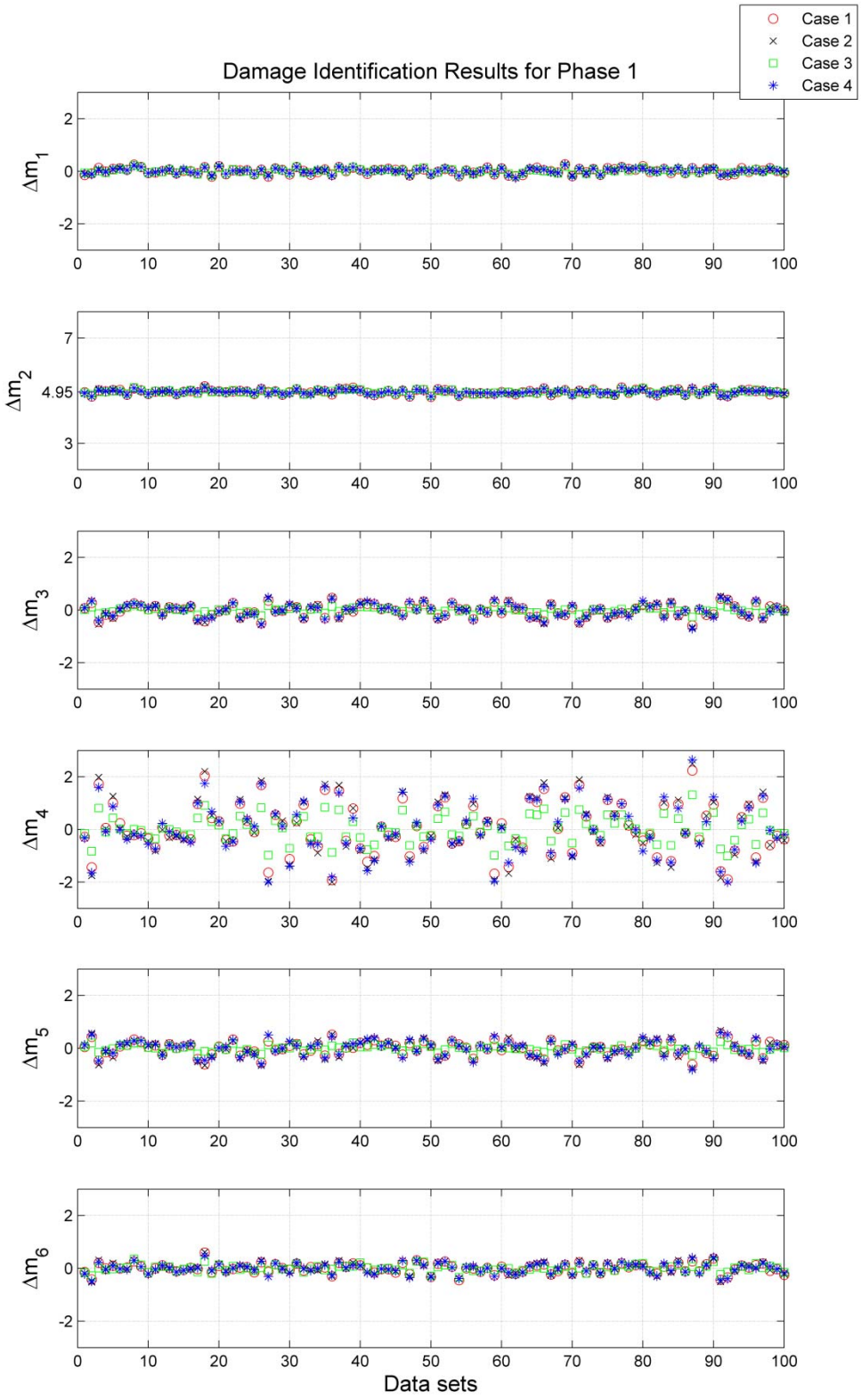

Figure 3.9 Damage identification results in Phase 1 (unit: kips)

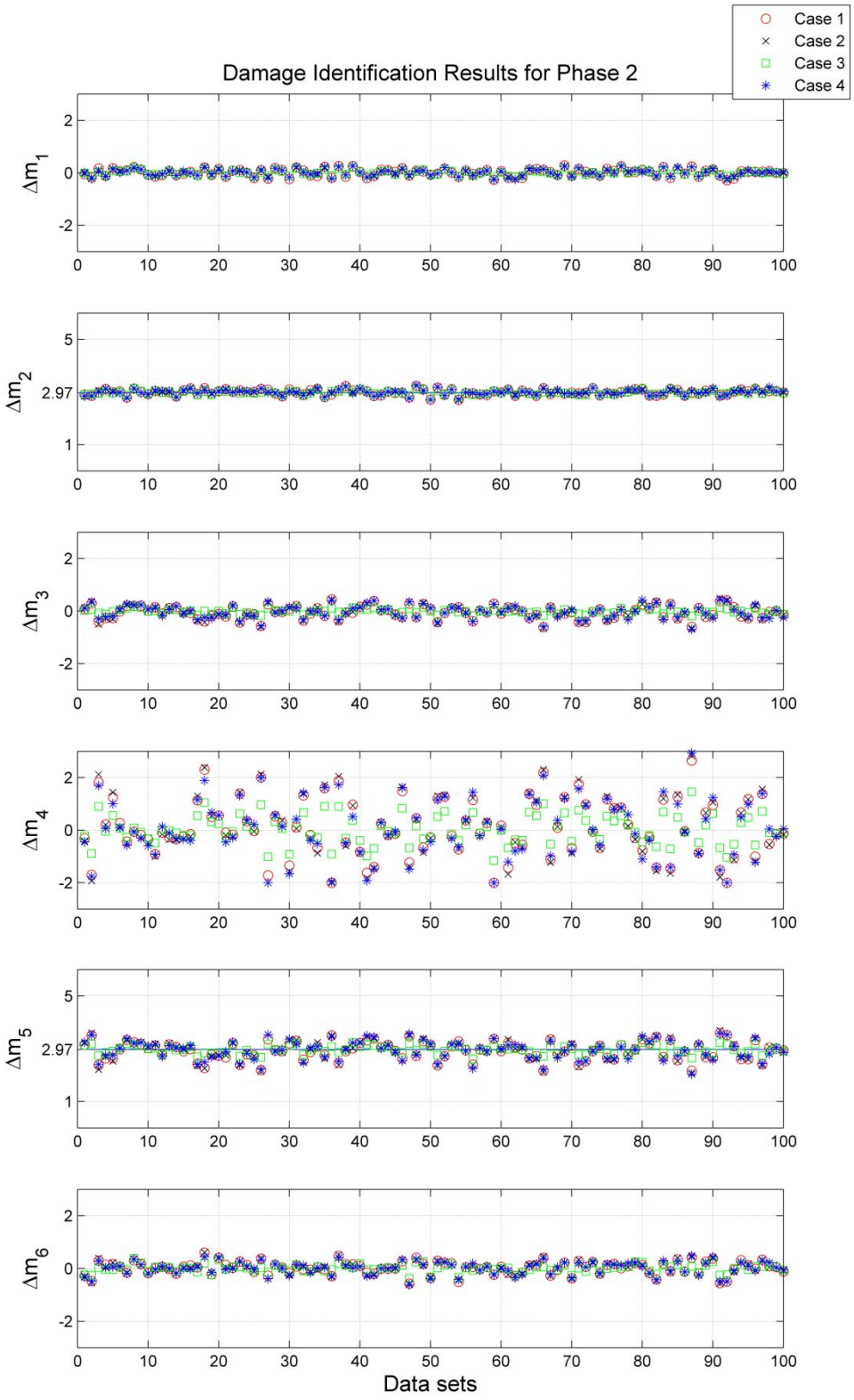

Figure 3.10 Damage identification results in Phase 2 (unit: kips)

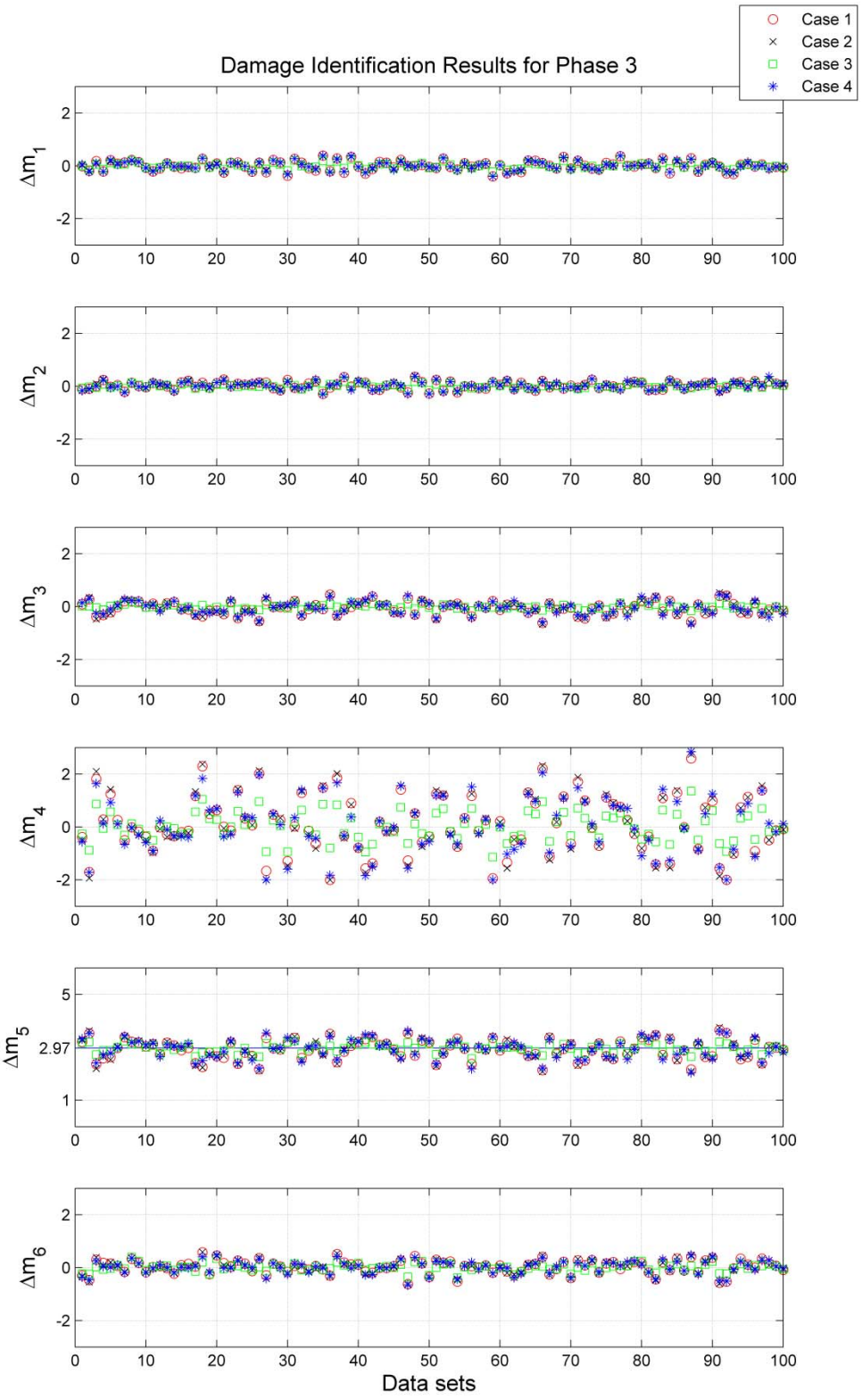

Figure 3.11 Damage identification results in Phase 3 (unit: kips)

3.4.4 *Analysis of Numerical Damage Identification Results*

Tables 3.4 to 3.6 (-5 to 7 kips bounds)

Overall all four cases of FE model updating were capable of accurately predicting the location and extent of simulated damage in the form of added mass on the FE model. The mean values for all identified Δm are very close to the exact masses loaded on the FE model in the presence of added noise.

Before the numerical damage identification was performed, we expected that increasing the number (8 accelerometers to 12 accelerometers) and types (accelerometers and strain gauges) of sensors would have a significant influence on improving the accuracy of FE model updating results, i.e., the identified results among the first three cases should get better, while the performance of Case 4 was expected to be worse than Case 3 due to the added noise.

A general trend of improvement can be found in the mean of identified values in Tables 3.4 to 3.6; however, the observed improvement is very small. The mean values of identified added masses in the 2nd and 3rd cases get closer to the exact value compared with the 1st case, while the mean values in Case 4 are between Cases 2 and 3. Thus, increasing the number and variety of sensors reduces the estimation bias. This improvement is more significant from Case 2 to Case 3 than from Case 1 to Case 2. The adverse influence of larger error in strain mode shapes is also verified by comparing Cases 3 and 4.

The variability of the identified results, however, will not reduce necessarily by adding more accelerometers as no reduction in standard deviations is observed from Case 1 to Case 2. Addition of strain gauges (from Case 2 to Case 3), however, significantly reduces the standard deviations. Moreover, the improvement in the results from Case 2 to Case 3 is more noticeable in substructure 2 (Δm_2) because strain gauges are located on the first three substructures. It should also be underlined that the largest variability is found in the estimated values of Δm_4. This can be explained by the fact that substructure 4 is on the top of Pier A, the middle support of the Dowling Hall footbridge, and has the smallest amount of vibration response (i.e., mode shape components). Therefore, the physical properties of this substructure are less sensitive to the identified vibration-based modal parameters.

Tables 3.7 to 3.9 (0 to 7 kips bounds)

As mentioned earlier, the first three cases of FE model updating are repeated while constraining the updating parameters to be positive and the results are reported in Tables 3.7 to 3.9. From these tables, it can be observed that in general the FE model updating is accurate in predicting the added mass. The results in these cases have slightly larger bias and smaller standard deviations when compared to the previously discussed results when the lower bounds are negative. Another noteworthy observation is the significant reduction in the standard deviation of Δm_5 from Case 1 to Case 2. This is mainly due to the fact that the extra four accelerometers in Case 2 are mounted on substructures 4, 5 and 6.

Information Gained through Model Updating

The information gained about the updating parameter from the considered measured data can be estimated as the change in the information entropy of the updating parameters. The relative information entropy/uncertainty of updating parameters is predicted as the trace of the logarithm of the Fisher Information Matrix, $\boldsymbol{Q}(\boldsymbol{\theta}) \approx \boldsymbol{J}_{\boldsymbol{\theta}}^{T}\boldsymbol{W}\boldsymbol{J}_{\boldsymbol{\theta}}$, as discussed in Section 2.7. The Jacobian matrix $\boldsymbol{J}_{\boldsymbol{\theta}}$ is constant when using the same combination of sensors and the weighting matrix $\boldsymbol{W}$ is dependent on COV of modal parameters. Thus, $\boldsymbol{W}$ is the deterministic factor to explain the difference between components of each column because the influence of noise is directly reflected in COVs. The lower the value of the information entropy, the more information the data provide to resolve the updating parameters. Table 3.10 reports the information entropy of all updating parameters considering four combinations of sensors and three noise scenarios. Condition of Noise (1) refers to the model updating Case 3 in which the COV of strain mode shapes are lower than displacement mode shapes while Noise (2) is corresponding to model updating Case 4 with strain mode shapes contaminated with higher noise.

Table 3.10 Information entropy values for different sensor and noise conditions

	8 Acc	12 Acc	12 Acc + 4 Sg	4 Sg
No Noise	11.4818	10.7486	10.6704	18.2696
Noise (1)	16.8175	16.9719	16.0776	18.9954
Noise (2)	16.8175	16.9719	16.9198	22.8662

From this table, it can be found that adding noise increases the value of entropy/uncertainty of updated model parameters. The difference between Noise (1) and Noise (2) is the considered error in strain mode shapes, so model updating cases with 8 and 12 accelerometers have the same values of entropy. Column 4 shows extremely large estimation uncertainties for updating parameters, since the four strain gauges are far less informative about the overall damage, as discussed in Section 2.4.3. In the absence of noise, all the modal parameters are equally accurate so their weights in the weighting matrix $\boldsymbol{W}$ are equal. Under this circumstance, increasing the number of accelerometers and addition of strain gauges reduce the entropy (1st row). However, when the modal parameters are noisy (2nd and 3rd rows), including more sensors does not necessarily provide more accurate estimates as it was observed in Section 3.4.3. This is due to the fact that the mode shape weights were adjusted to have the same normalized sum when increasing the number of accelerometers from 8 to 12, and therefore larger COV/uncertainty was considered for the 12-sensor configuration. It is also observed that when the noise in strain measurement is relatively small (Noise 1), addition of strain gauges reduces the entropy. However, when the strain mode shapes have larger error (Noise 2), addition of strain gauges does not improve the accuracy of updating results. The findings from the information gain study are consistent with the obtained model updating results in previous section, justifying the occasional increase in the variability of updating parameters when going from 8 accelerometers to 12 accelerometers.

This type of information gain study can quantify the influence of increasing number and type of sensors with considered noise conditions on model updating results. It is important to perform such study in the instrumentation design for vibration-based SHM. Of course, the information gain study can also be performed more accurately in a Bayesian framework formulation as proposed by Jayne (1978).

3.5 Damage Identification Using Experimental Data

3.5.1 *Reference Model*

The first step in the application of FE model updating for damage identification based on experimental data is calibration of the initial FE model to a reference model that represents the undamaged condition of the structure. Modal parameters of the bridge have been identified before and during the three phases of the loading and reported in Section 3.3. The reference model was calibrated based on the reference modal parameters corresponding to the data measured at 11:00 am, May 31, 2013, five hours before the beginning of the loading tests. The updating parameters are selected as stiffness of elements composing the considered six substructures in the FE model (Figure 2.5). Other physical properties of the model are kept as indicated in the design drawings and the initial model. The calibration is performed to match the modal parameters of the reference model and reference modal parameters identified from measured data.

Section 3.3 reports the identified natural frequencies of the bridge from the ambient acceleration data before and during the load testing. From Figure 3.7 and

previous system identification studies on this footbridge, it is observed that the natural frequencies of modes 1, 3 and 4 are accurately identified, frequencies of modes 5 and 6 have very large estimation errors, and mode 2 is often missed in the identification. Modes 2, 5, and 6 have considerably smaller impact on the updating parameters than modes 1, 3, and 4. Therefore, the weight assigned to each mode in the model updating is decided. The considered weights for the six identified modes in this study are reported in Table 3.11.

Table 3.11 Weighting factors for 1st six modes

w_1	w_2	w_3	w_4	w_5	w_6
1.0	0.01	1.0	1.0	0.01	0.01

Table 3.12 displays the damage factors obtained for the six substructures of reference model. Table 3.13 compares the modal parameters of the reference model with the identified reference modal parameters. MAC values were calculated using mode shapes consisting of 12 components corresponding to the 12 accelerometers. It can be found that modal parameters of mode 1, 3 and 4 match their identified counterparts well while modes 5 and 6 of the updated FE model do not match the data. This can be due to the larger estimation errors of these modes and the lower weights assigned to them in the model updating process.

Table 3.12 Damage factors for the reference model

	a_1	a_2	a_3	a_4	a_5	a_6
Damage factor	-0.0782	0.3235	-0.2363	-0.1374	0.0592	-0.0260

Table 3.13 Modal parameters of the reference model compared with identified modal parameters

	Natural frequency (Hz)		MAC (%)
	Identified	Reference Model	
Mode 1	4.65	4.63	99
Mode 2	6.21	6.12	100
Mode 3	7.05	7.05	99
Mode 4	8.90	8.94	100
Mode 5	13.08	13.52	91
Mode 6	13.58	13.81	95

3.5.2 *FE Mode Updating Results*

Three cases of FE model updating were performed for each loading phase, namely Case 1: using experimental data from eight accelerometers (Figure 1.3, a), Case 2: using data from twelve accelerometers (Figure 1.4, old accelerometers plus A9 to A12) and Case 3: using data measured by twelve accelerometers and three (one strain gauge did not work) strain gauges (Figure 1.4, all the sensors) to identify the damage (added mass) on six segments of the Dowling Hall bridge. Due to malfunction of strain gauge SF4, only three strain gauges were in service during the tests. Therefore, the strain mode shape residuals only have two components after one of the three components is selected as reference. In addition, the experimental strain measurements were found to be noisy and could not match well with their FE model counterparts. Therefore, Case 3 results are excluded from the reported experimental damage identification results in this chapter.

After removing the incomplete and outlier sets of identified modal parameters, 119 data sets remained for Phase 1, 116 data sets were left for Phase 2, and 107

data sets for Phase 3. Two cases of FE model updating (Cases 1 and 2) were then performed using each set of identified modal parameters resulting in a total of 2 x (119 + 116 + 107) = 684 updating runs. The six updating parameters were constrained between 0 and 8 kips for Phase 1 and bounded between 0 and 5 kips for Phases 2 and 3. The statistics of the updated added mass for different substructures are reported in Tables 3.14 to 3.16 and Figures 3.12 to 3.14 for both cases of instrumentation and the three phases of loading.

Table 3.14 Statistics of identified added mass in Phase 1 (experimental)

Phase 1		Δm_1	Δm_2	Δm_3	Δm_4	Δm_5	Δm_6
Exact (kips)		**0**	**4.95**	**0**	**0**	**0**	**0**
Mean (kips)	Case 1	0	4.5556	0	0	1.5307	0.0318
	Case 2	0	5.4283	0	0	1.0393	0.0125
Std (kips)	Case 1	0	0.4909	0	0	0.5649	0.1343
	Case 2	0	0.4759	0	0	0.5106	0.0673

Table 3.15 Statistics of identified added mass in Phase 2 (experimental)

Phase 2		Δm_1	Δm_2	Δm_3	Δm_4	Δm_5	Δm_6
Exact (kips)		**0**	**2.97**	**0**	**0**	**2.97**	**0**
Mean (kips)	Case 1	0	2.9374	0	0.1180	2.7897	0.1161
	Case 2	0	2.9333	0	0	2.7242	0.0450
Std (kips)	Case 1	0	0.4528	0	0.8996	0.3387	0.2937
	Case 2	0	0.4502	0	0	0.3281	0.1719

Table 3.16 Statistics of identified added mass in Phase 3 (experimental)

Phase 3		Δm_1	Δm_2	Δm_3	Δm_4	Δm_5	Δm_6
Exact (kips)		**0**	**0**	**0**	**0**	**2.97**	**0**
Mean (kips)	Case 1	0	0.6139	0	2.7134	2.1551	0.4654
	Case 2	0	0.0813	0	0.4308	3.1496	0.2357
Std (kips)	Case 1	0	0.7626	0	2.4175	1.0757	1.3891
	Case 2	0	0.3578	0	0.7870	0.6546	0.4790

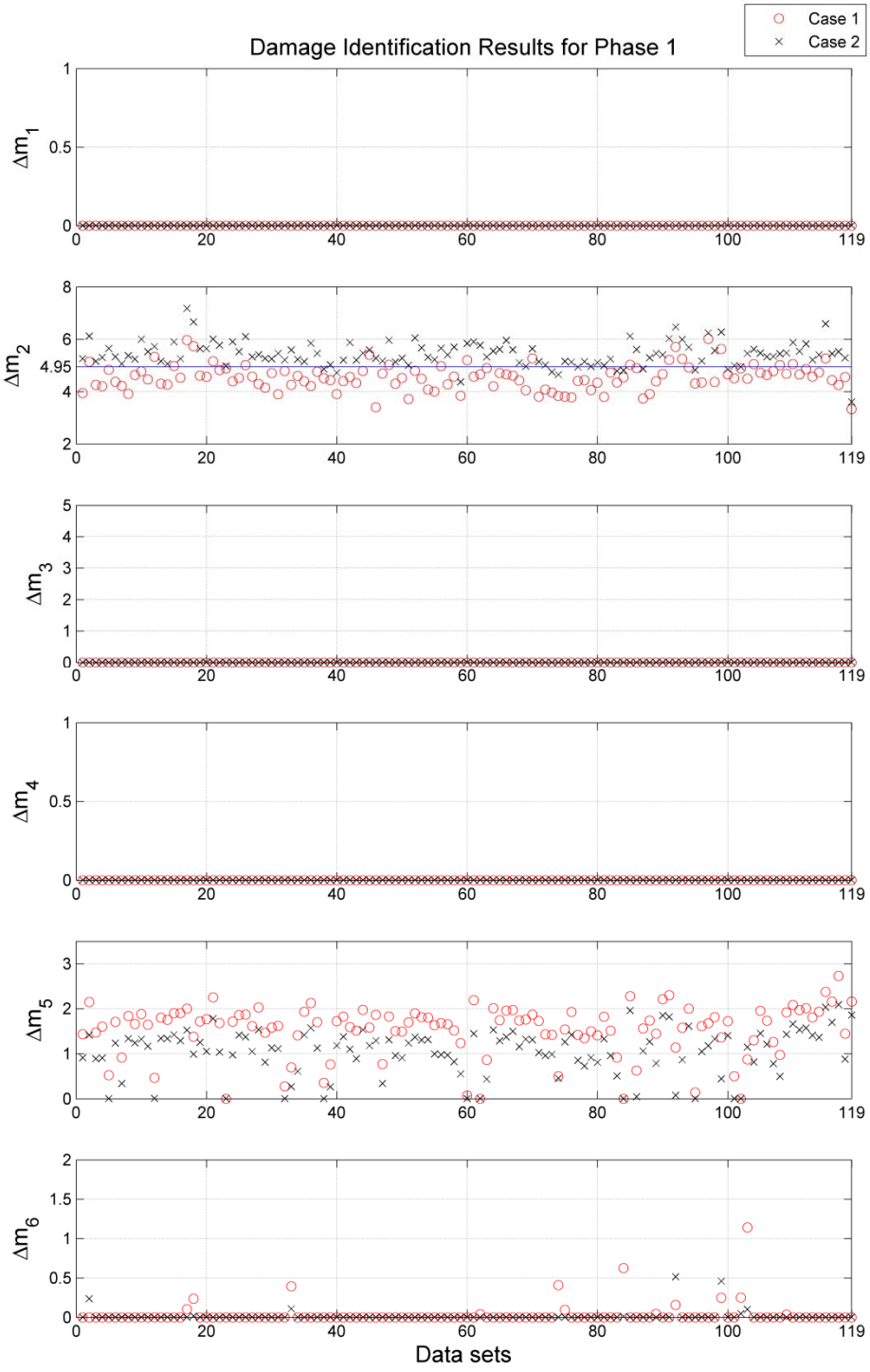

Figure 3.12 Experimental damage identification results in Phase 1 (unit: kips)

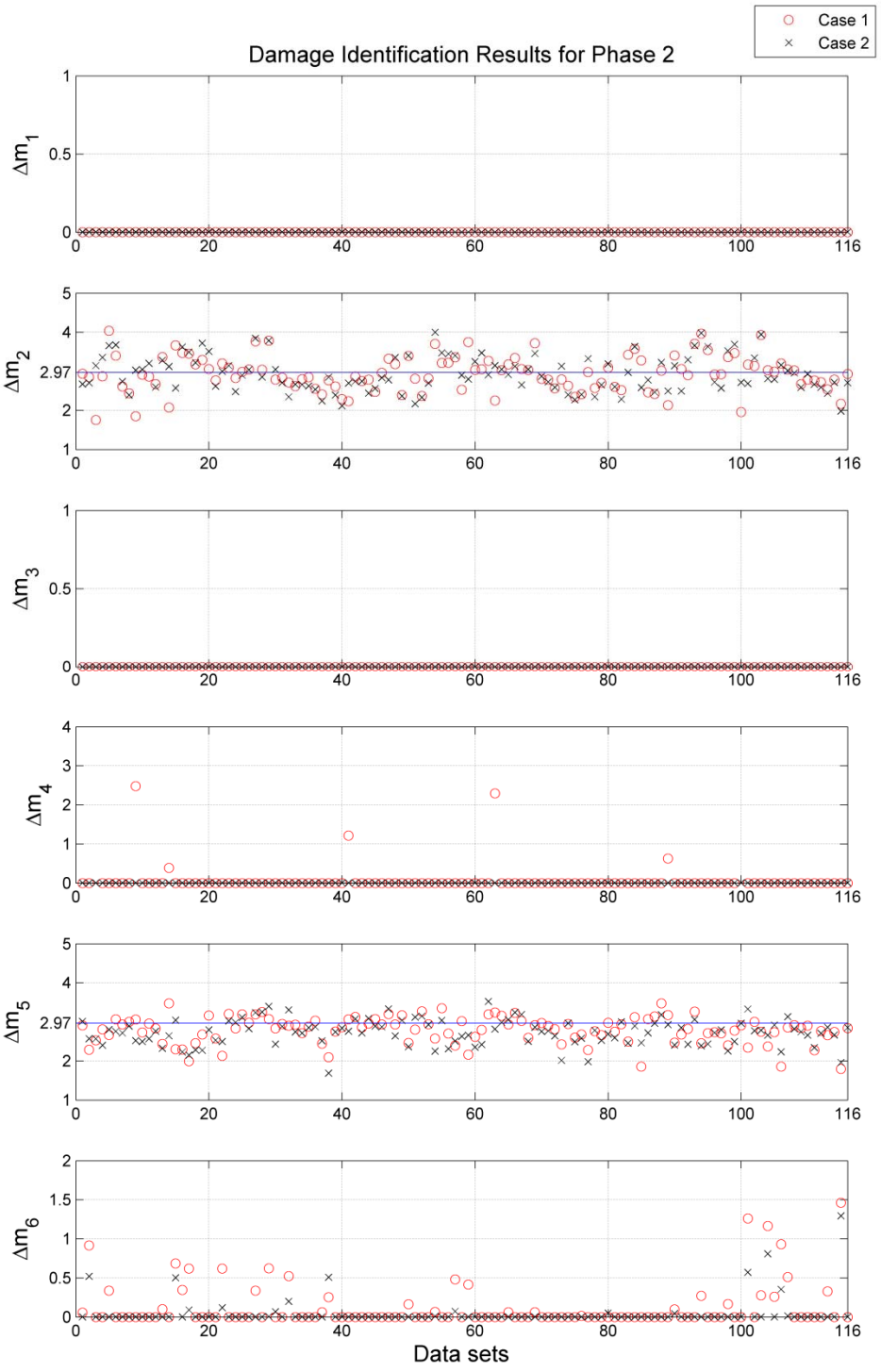

Figure 3.13 Experimental damage identification results in Phase 2 (unit: kips)

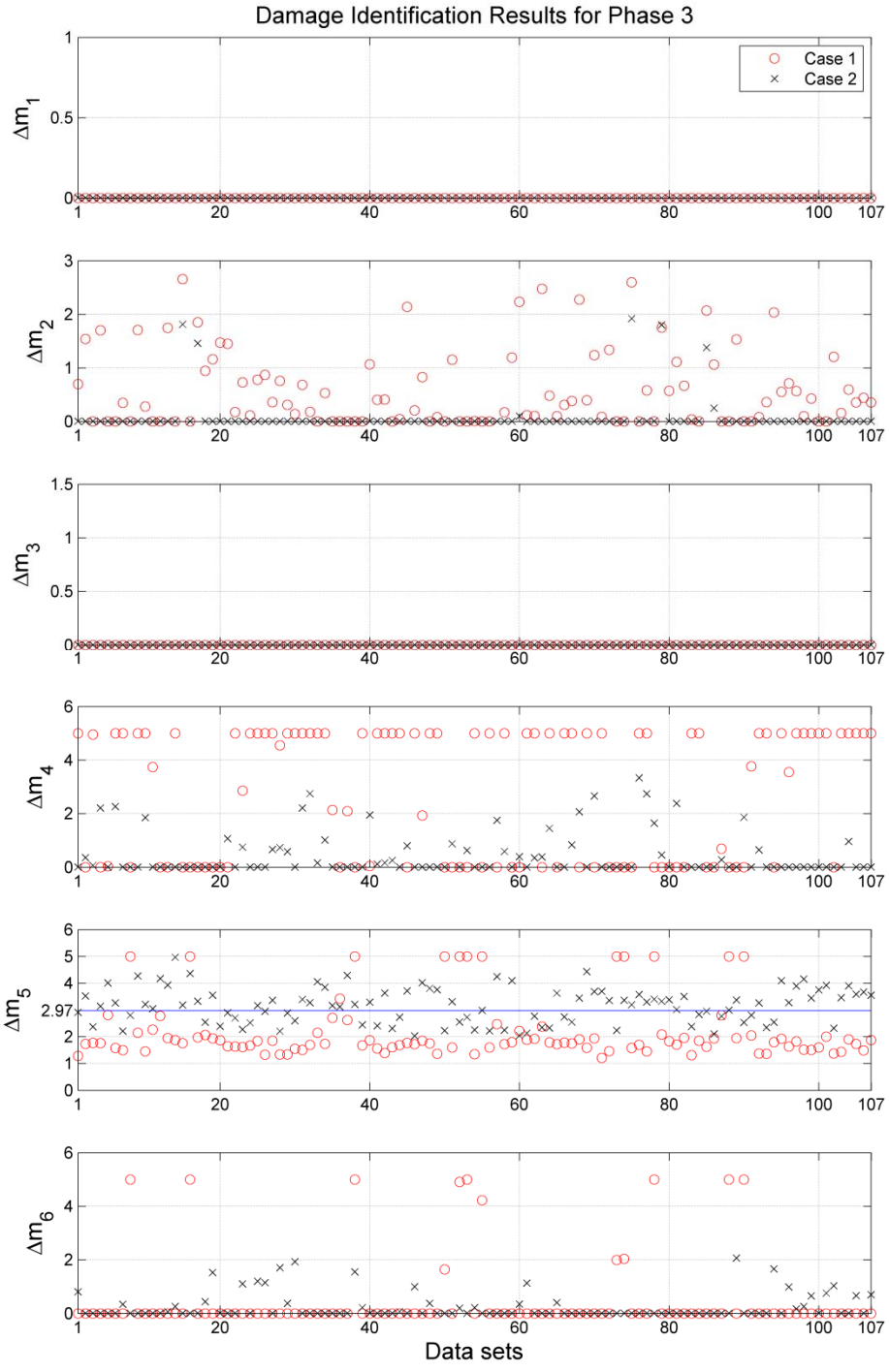

Figure 3.14 Experimental damage identification results in Phase 3 (unit: kips)

3.5.3 *Analysis of Experimental Damage Identification Results*

Phase 1

Table 3.14 presents the statistical properties of the identified added masses for Phase 1. The improvement by using more accelerometers can be found in Δm_5 and Δm_6 as their estimation bias is reduced from Case 1 to Case 2. However, such improvement does not exist for Δm_2, and model updating Case 1 provides smaller bias than Case 2. It is also found that Δm_5 is identified with the largest variability/uncertainty and bias. This can be due to the fact that substructure 5 has similar sensitivities to the natural frequency residuals as substructure 2, and only mode shape residuals provide independent information about these two updating parameters. Therefore small errors in mode shape residuals can cause significant estimation error in Δm_5. This fact can also explain why the identified values of Δm_2 are nonzero in Phase 3.

In this phase, Δm_4 is found to be zero consistently for both cases of updating, which is not observed in the other phases. Finally, it is observed that Δm_6 estimates have the largest improvements with addition of the four accelerometers from Case 1 to Case 2 which makes sense since three of the added accelerometers are located at boundaries of substructure 6.

Phase 2

From Table 3.15, it is found that this phase of loading can also be quite accurately identified in the two cases on model updating. Δm_2 is identified with very small bias but rather larger variability, while Δm_5 estimates have larger bias and very small variability. The estimation bias and uncertainty/variability is reduced in

these two substructures by using more sensors (Case 1 to Case 2) but this reduction is very small. On the other hand, the reduction in bias and variability of Δm_4 and Δm_6 is significant with addition of 4 accelerometers. Therefore, in Phase 2 when there is added mass on substructure 5, Case 1 is not able to accurately estimate the added masses on substructures 4 and 6 since only two sensors were mounted on segments 4 to 6 (Figure 1.3, a). Equipped with 4 extra sensors, Case 2 accurately predicted the masses added on substructures 4 and 6. The model updating results of Δm_4 and Δm_6 in Phase 2 have confirmed the advantages of including more sensors for localization of damages.

Phase 3

Table 3.16 reports the identified damage (mass) during the last phase of load testing. This table provides more convincing evidence on how the added sensors on the Dowling Hall side of the footbridge can drastically improve the damage identification results when damage is located on this side of the bridge. For Case 1, the updating factors are less accurate especially for substructures 4 and 6 and for certain data sets the added mass estimates reach the upper bound of 5 kips as seen in Figure 3.14. It can be concluded that data from the 8 accelerometers do not provide adequate information for identification of considered damage scenario. However, the updating results in Case 2 are drastically improved and the updating results for these two substructures are generally acceptable.

3.6 Conclusion

In this chapter, performance of FE model updating for identification of damage on the Dowling Hall Footbridge is evaluated using numerical and experimental data. In the numerical study, three damage scenarios and four instrumentation setups were considered. In all cases, location and extent of simulated damage as the added mass on different segments of the bridge deck are identified accurately. The accuracy of identification results is improved by adding the number of sensors in the absence of noise. However, when noisy data is used, increasing the number of sensors will not necessarily improve the model updating results. The results highly depend on the quality of data from added sensors. It is also found that the stain gauges will provide more information about damage close to the locations of sensors while do not necessarily improve the estimation accuracy of farther located substructure parameters.

In the experimental study, model updating could only be performed using two instrumentation setups, Case 1 and Case 2, as the identified strain mode shapes could not be matched well with the model. In general, both cases of model updating can identify the simulated damage reasonably well during Phases 1 and 2. The mean updating values for substructures where masses were added are close to the exact values taking into account the existence of not only measurement noise and modal identification errors, but also modeling errors. In Phase 3 of loading, only Case 2 of model updating can successfully identify the damage on substructure 5. It indicates the lack of sufficient information in the measured data

in Case 1. In all three phases, the standard deviations of updating parameters decrease from Case 1 to Case 2, however, this reduction is most significant in Phase 3. It is also observed that the updating parameters Δm_1 and Δm_3 are always estimated at their exact value of zero. This is due to the fact that 6 sensors were attached on the first three segments throughout the test, and that these updating parameters are clearly observable from the measured data. On the other hand, Δm_6 is estimated with large bias in all cases and loading scenarios. This phenomenon can be due to the fact that the signal-to-noise ratio of measurements from accelerometers close to this substructure are smaller given their longer cables and also due to the more complicated boundary condition at the Dowling Hall end of the bridge causing larger modeling errors.

Chapter 4 Conclusions and Future Works

4.1 Summary and Conclusions

This thesis focuses on the damage identification of the Dowling Hall footbridge at Tufts University campus using the ambient measured data from accelerometers and strain gauges. Performance of FE model updating for estimation of simulated damage on the bridge is studied when applied to numerically simulated data as well as experimentally measured data. Within each application, three damage scenarios are considered using various instrumentation setups to examine the effect of number, location and type of sensors.

In the application of FE model updating on numerically simulated data, influence of uncertainty caused by measurement error and estimation inaccuracy of modal parameters was simulated in the form of added noise to modal parameters. However, effects of modeling errors were not considered in this numerical study. Overall, the sensitivity-based FE model updating method could successfully identify the simulated damage on each substructure using the noise-polluted data. The identification results illustrate that the noise, or in other words, the quality of the measured data plays an important role on the accuracy of the damage identification results. When the noise in measurement data is small, adding more accelerometers and strain gauges improves the updating results. However, when data from additional sensors are noisier, usage of more sensors will not necessarily yield better results. Moreover, it is observed that use of additional

accelerometers and especially strain gauges has the largest impact on estimation accuracy of model parameters of segments where the sensors are located. It should be noted that the strain gauges will only provide information about the part of the structure close to its location.

In the experimental application, modal parameters are extracted from measured ambient vibration response of the actual bridge under different simulated damage (as added mass) scenarios. In this application, influence of modeling errors, measurement noise, and estimation error is no longer controllable. The number and location of accelerometers become key factors that affect the accuracy of damage identification results. However, the updating results demonstrate that the improvement brought by new sensors is evident mainly in results of damage happening near the location of these sensors. It is found that when the mass is added on a section of bridge with no sensors, the model updating procedure fails to detect the simulated damage correctly. Successful identification results are obtained when using newly installed sensors near the location of damage. It shows that the instrumentation design plays an important role in the success of damage identification through FE model updating. The experimental application further verifies the addition of accelerometers will improve the accuracy in localizing and quantifying damage.

4.2 Future works

The following suggestions and extensions for the future research are made:

- Currently there are 12 accelerometers and 4 strain gauges working on the footbridge, most of which are located on substructure 1 to 4. More sensors need to be mounted on the Dowling Hall side of the bridge. Larger numbers of accelerometers and strain gauges with better performance would allow more accurate and refined damage identification of this bridge.
- All the current sensors on the bridge are connected to the data acquisition device by wires. Use of wireless sensors can potentially reduce the noise in experimental modal parameters.
- Study the effects of modeling errors. The FE model used in this research is based on multiple assumptions for simplification. Effects of using a more sophisticated FE model in model updating should be investigated numerically.
- In this project, natural frequencies and mode shapes of the 1st six modes are extracted from the experimental data and used for model updating. Larger number of vibration modes can be identified from the data and included in the model updating.
- Environmental variables such as temperature, humidity and wind speed are not accounted for in this project. Effects of these variables on identified modal parameters and subsequent model updating can be studied. Note that the temperature effects on FE model updating of the Dowling Hall footbridge have been investigated by Moaveni and Behmanesh (2012) in the absence of simulated damage in the bridge.

References

Allemang, R. J. and Brown, D. L. (1982). "A correlation coefficient for modal vector analysis." *In Proceedings of IMAC I: 1st International Modal Analysis Conference*, pages 110–116, Orlando, Florida.

American Society of Civil Engineers (ASCE) (2013). "Report Card for America's Infrastructure." <http://www.infrastructurereportcard.org/>.

Bowman, J. (2003). *Vibration Testing and Modal Identification of the Dowling Hall Footbridge at Tufts University.* Master Thesis, Department of Civil and Environmental Engineering, Tufts University, Medford, Massachusetts.

Brownjohn, J. M. W., Moyo, P., Omenzetter, P. and Lu, Y. (2003). "Assessment of highway bridge upgrading by dynamic testing and finite-element model updating." *Journal of Bridge Engineering*, **8**(3):162–172.

Conte, J. and Liu, M. (2000). *Use of Long-Gage Fiber Optic Sensors for Earthquake Response Monitoring and Non-Destructive Evaluation of Structures.* A Report on Research Sponsored by Kajima Corporation, Department of Civil & Environmental Engineering University of California at Los Angeles, California.

Dawson, B. (1976). "Vibration condition monitoring techniques for rotating machinery." *The Shock and Vibration Digest* (London: SpingerLink) **8** (12): 3.

Doebling, S. W., Farrar, C. R. and Prime, M. B. (1998). "A summary review of vibration-based damage identification methods." T*he Shock and Vibration Digest*, **30**(2), 99–105.

Doebling, S. W., Farrar, C. R., Prime, M. B. and Shevitz, D. W. (1996). "Damage identification in structures and mechanical systems based on changes in their vibration characteristics: A detailed literature survey." *Los Alamos National Laboratory Rep. No. LA-13070-MS*, Los Alamos, NM.

Filippou, F.C. and Constantinides, M. (2004). "FEDEASLab getting started guide and simulation examples." *Technical Report NEESgrid-2004-22*, Available from: http://fedeaslab.berkeley.edu.

Fox, R. and Kapoor, M. (1968). "Rate of change of eigenvalues and eigenvectors." *AIAA Journal*, 6:2426–2429.

Friswell, M. I. and Mottershead, J. E. (1995). *Finite Element Model Updating in Structural Dynamics*. Kluwer Academic Publishers, Dordrecht, the Netherlands.

Jaynes, E.T. (1978). "Where do we stand on maximum entropy?" in: R.D Levine, M. Tribus (Eds.), *The Maximum Entropy Formalism,* MIT Press, Cambridge, MA.

Kody, A. (2013). *Simulation and Detection of Damage on the Dowling Hall Footbridge.* Research Credit Paper, Department of Civil and Environmental Engineering, Tufts University, Medford, Massachusetts.

Kody, A. and Moaveni, B. (2011). *Simulation of Structural Damage on the Dowling Hall Footbridge.* Summer Scholar Report, Department of Civil and Environmental Engineering, Tufts University, Medford, Massachusetts.

Link, M. (1999) "Updating of analytical models - Review of numerical procedures and application aspects." *Proceedings of the Structural Dynamics Forum SD2000*, Los Alamos.

Moaveni, B. and Behmanesh, I. (2012). "Effects of Changing Ambient Temperature on Finite Element Model Updating of the Dowling Hall Footbridge." *Engineering Structures*, 43, 58-68.

Moaveni, B., He, X. and Conte, J. P. (2008). "Damage Identification of a Composite Beam Using Finite Element Model Updating." *Computer-Aided Civil and Infrastructure Engineering*, **23** (2008): 339–359.

Moser, P. (2010). *Continuous Monitoring of the Dowling Hall Footbridge*. Master Thesis, Department of Civil and Environmental Engineering, Tufts University, Medford, Massachusetts.

Moser, P. and Moaveni, B. (2013). "Design and deployment of a continuous monitoring system for the Dowling Hall Footbridge." *Experimental Techniques*, **37**(1), 15-26.

Papadimitriou, C. (2004). "Optimal sensor placement for parametric identification of structural systems." *Journal of Sound and Vibration*, 278, 923–947.

Peeters, B. and De Roeck, G. (1999). "Reference-based stochastic subspace identification for output-only modal analysis." *Mechanical Systems and Signal Processing*, **13** (6), 855-878.

Rytter, A. (1993). *Vibration Based Inspection of Civil Engineering Structures*. Ph.D. Dissertation, Department of Building Technology and Structural Engineering, Aalborg University, Denmark.

Sanayei, M. and Saletnik, M. (1996). "Parameter Estimation of Structures from Static Strain Measurements. I: Formulation." *Journal of Structural Engineering*, Vol. 122, No. 5, May, 1996.

Skift.com, http://skift.com/2013/05/25/bridge-collapse-shows-lack-of-support-for-infrastructure-improvements, "Washington State bridge collapse highlights aging U.S. infrastructure." Downloaded on July 25, 2013.

Teughels, A. (2003). *Inverse Modeling of Civil Engineering Structures Based On Operational Modal Data*. PhD Thesis, Department of Civil Engineering, K.U. Leuven, Belgium.

Van Overscheen, P. and De Moore, B. (1996). *Subspace identification for linear systems*, Kluwer Academic Publishers, Massachusetts.

Zhang, Q. W., Chang, C. C. and Chang, T. Y. P. (2000). "Finite element model updating for structures with parametric constraints." *Earthquake Engineering and Structural Dynamics*, 29:927–944.

Zhang, Q. W., Chang, T. Y. P. and Chang, C. C. (2001). "Finite-element model updating for the Kap Shui Mun cable-stayed bridge." *Journal of Bridge Engineering*, **6**(4): 285–293.